




Effects of finite counterion size and nonhomogeneous permittivity and viscosity of the solution on the electrokinetics of a concentrated salt-free colloid

F. Carrique **Departamento de Física Aplicada I, Facultad de Ciencias, Universidad de Málaga, 29071 Málaga, Spain*E. Ruiz-Reina †*Departamento de Física Aplicada II, Institute Carlos I for Theoretical and Computational Physics (iCI), Universidad de Málaga, 29071 Málaga, Spain*F. J. Arroyo ‡*Departamento de Física, Facultad de Ciencias Experimentales, Universidad de Jaén, 23071 Jaén, Spain*J. J. López-García §*Departamento de Física, Facultad de Ciencias Experimentales, Universidad de Jaén, 23071 Jaén, Spain*A. V. Delgado ||*Departamento de Física Aplicada, Facultad de Ciencias, Universidad de Granada, 18071 Granada, Spain*

(Received 26 February 2024; accepted 4 June 2024; published 1 July 2024)

In the present work, a general model of the electrokinetics and dielectric response of a concentrated salt-free colloid is developed which includes consideration of the finite size of the counterions released by the particles to the solution, a nonhomogeneous permittivity of the solution, the existence of Born and dielectrophoretic forces acting on the counterions, and especially the fact that the solution viscosity and diffusion counterion coefficient are allowed to be functions of the local counterion concentration. These effects have recently been discussed by J. J. López-García *et al.* [*Phys. Rev. Fluids* **4**, 103702 (2019)] in the case of dilute colloids in general electrolyte solutions. The objective of this work is to explore the new effects and their influence on the electrokinetic response of concentrated salt-free systems. Present results confirm previous findings regarding the important increases of the dc electrophoretic mobility and dc electrical conductivity, as well as huge increments of the dynamic electrophoretic mobilities at high frequencies when finite-ion-size effects were taken into account. In addition, consideration of the viscosity of the solution and of the counterion diffusion coefficient as functions of the local counterion concentration leads to a decrease of the magnitude of the previous electrokinetic results. The theory incorporates a more convenient hard-sphere hydrodynamic model to account for the nonhomogeneous viscosity of the solution than others proposed in previous works in the literature. A comparison is elaborated on between electrokinetic and dielectric responses with different levels of complexity of the theoretical model, starting from the case of pointlike counterions and following with the inclusion in sequence of additional aspects such as finite counterion size, nonhomogeneous electrical permittivity with associated Born and dielectrophoretic effects, and, finally, position-dependent viscosity and diffusion counterion coefficient, and clearly shows the influence of individual effects on the general electrokinetic response and especially the relevant role the nonhomogeneous viscosity on the dc and ac electrokinetic behavior of salt-free colloids.

DOI: [10.1103/PhysRevE.110.014601](https://doi.org/10.1103/PhysRevE.110.014601)

I. INTRODUCTION

A salt-free colloid is a system composed of charged particles dispersed in aqueous or nonaqueous solutions in the absence of any added salt. Because of neutrality an exact countercharge is developed, typically in the form of counterions released by the particles to the solution as they become

charged in such a solution. These systems have been less studied than those in general electrolyte solutions, mainly when the concentration of particles is such that the system is far from being considered as dilute. In these situations, salt-free colloids can form ordered phases giving rise to the formation of colloidal crystals at even low particle concentrations. In salt-free colloids the screening effect of ionic species in solution on the particle charge is comparatively low and the long-range repulsive forces between particles facilitate the formation of such crystals [1]. Another important aspect that is attracting experimental and theoretical attention is the study of the condensation layer of counterions that develops close to the surfaces of the particles in salt-free colloids beyond a

*Contact author: carrique@uma.es†Contact author: eruir@uma.es‡Contact author: fjarroyo@ujaen.es§Contact author: jjgarcia@ujaen.es||Contact author: adelgado@ugr.es

critical particle surface charge density [2–4]. This counterion condensation effect has a large influence in general soft matter and only takes place in very low-salt systems, mainly in pure salt-free ones [5].

In recent years the present and other authors have explored the electrokinetic and dielectric response in dc and ac electric fields of concentrated salt-free colloids by assuming in a first instance that the released counterions can be treated as pointlike [6–9]. Many studies have shown that the consideration of finite size for the ions in solution is crucial to gain a more realistic picture of these systems leading to a better understanding of the mentioned responses [4,10–13]. Accounting for the finite ion size, the counterion concentrations near the particle surfaces can no longer reach the unrealistic values attained when they are considered pointlike.

This issue was addressed by the authors in a recent paper [14] by using hard-sphere model approaches by Carnahan and Starling [15] and by a simpler one by Bikerman [16], but quite recently it has been argued that many important properties that are classically considered to maintain constant values in these electrokinetic studies have to be revised [10,17,18]. The finite size of the ions not only leads to steric effects but also to a modification of properties as the electrical permittivity of the solution, since ions occupy a certain volume that is not available for the liquid solution. Likewise, the ions have also been considered as charged dielectric spheres with a different permittivity as that of the solution [17]. This provokes the existence of new forces acting on the counterions (Born and dielectrophoretic forces) in addition to the electrical, thermal, and steric ones, as it has been recently pointed out by López-García *et al.* [19]. In those works, it is emphasized that the presence of ions of finite size in the solution should lead to the enhancement of the solution viscosity with the increase of ion concentration and, therefore, to a nonhomogeneous dependence of permittivity and viscosity with the distance from the surface of the particle. This aspect is quite relevant to us considering the huge counterion concentration that occurs in the neighbourhood of the particle surface especially when this is highly charged. In summary, the permittivity and viscosity of the solution, and consequently the counterion diffusion coefficient, should be functions of the local counterion concentration recovering their bulk values in the solution far from the charged particle surfaces. The mentioned authors have shown that for dilute colloids in general electrolyte solutions the consideration of finite ion size and Born and dielectrophoretic forces acting on the ions because of the solution permittivity dependence with the local ion concentration, give rise to enhancements of different electrokinetic properties, such as the particle electrophoretic mobility or the electric permittivity of the colloid. On the contrary, they have also shown that an increase of the viscosity might have an opposite effect on the electrophoretic mobility, partly neutralizing those enhancements. This has been demonstrated in their previous work [19], which to our knowledge is the first study addressing all the latter aspects. In the present work, their approach will be for the first time applied to concentrated salt-free colloids. López-García *et al.*'s work is focused on dilute suspensions in salt-added solutions, and, in addition, they use the finite ion-size model by Boublik-Mansoori-Carnahan-Starling-Leland [20,21] which allows for multiple ionic species having

different ionic sizes, a feature not significant to our work, as only one ionic species is considered. Furthermore, the Batchelor-Green equation [22] chosen in Ref. [19] to account for the viscosity of the nonhomogeneous electrolyte will not be used because it seems to underestimate the local viscosity. Instead, use will be made of a result which is a simplification for hard spheres (a rough and simple but useful approximation for the counterions in the systems considered in this work, modeled as charged dielectric spheres) of a previously reported cell model of the electroviscous effect of moderately concentrated colloidal suspensions [23] (RR&C model hereafter, see also the excellent work by Zholkovskiy *et al.* where the cell model is analyzed in the frame of a more general hydrodynamic viscosity model [23]). The complete RR&C electroviscous model is built on the basis of a hard-sphere model to which electroviscous effects have been incorporated. The RR&C hard-sphere model coincides with a particular case of the hydrodynamic hard-sphere model by Simha [24] with a special condition by Happel [25] on the size of the cell. This aspect will be studied in more detail in Sec. V.

In the present work, attention will be paid not only to the equilibrium double-layer properties and response to dc electric fields but also the complex dynamic electrophoretic mobility, the electrical conductivity, and electrical permittivity of the concentrated salt-free colloid in ac electric fields (the response in dc electric fields is also attained when the frequency of the ac electric field is made zero). To that aim the paper is structured as follows. First, the equilibrium case (electrical potential and counterion concentration versus distance to the particle surface) will be studied with all the relevant effects included. Second, the general case of the electrokinetic and dielectric response of a concentrated salt-free colloid will be addressed, separating it into two aspects: the general one with all the effects included and a simpler one with just steric and Born and dielectrophoretic forces taken into account for comparison (nonhomogeneous viscosity and nonhomogeneous diffusion counterion coefficient excluded) in order to improve the discussion regarding the new effects.

II. EFFECTS OF THE FINITE COUNTERION SIZE AND NONHOMOGENEOUS ELECTRICAL PERMITTIVITY ON THE EQUILIBRIUM STRUCTURE OF THE EDL

In this section we will study the effect at equilibrium of all the relevant aspects mentioned in the previous section. As in a recent paper [14] the excluded volume of ions in a salt-free colloid will be addressed by considering a Carnahan-Starling activity coefficient γ_{CS}^0 of the counterions released from the particles to the solution and also for comparison by a Bikerman-like activity coefficient γ_{Bk}^0 depending on the packing fraction of counterions (hereafter the superindex “0” will refer to an equilibrium quantity). As in previous studies, use will be made of a spherical cell model (the Kuwabara cell model [26]) to manage, in an average way, the particle-particle electrohydrodynamic interactions in the colloid, with especial relevance when it is highly concentrated. A spherical cell is composed of one particle of radius a at its center that is surrounded by a concentric sphere of solution of radius b . This outer radius will be determined by making the particle volume fraction calculated with a single cell coincident with that

of the entire colloid ϕ : $\phi = (a/b)^3$. The Carnahan-Starling activity coefficient γ_{CS}^0 of the released counterions is given by [15]

$$\gamma_{CS}^0(r) = \exp\left(\frac{\varphi^0(r)\{8 - 9\varphi^0(r) + 3[\varphi^0(r)]^2\}}{[1 - \varphi^0(r)]^3}\right), \quad (1)$$

where $\varphi^0(r)$ is the counterion volume fraction at a radial distance r from the center of the particle, and it can be related to the counterion concentration $n^0(r)$ as:

$$\varphi^0(r) = n^0(r)V_c = n^0(r)\frac{4}{3}\pi R^3, \quad (2)$$

where V_c is the volume of a spherical counterion of radius R .

On the other hand, the Bikerman activity coefficient γ_{Bk}^0 of the counterions, allowing for different packing fractions, is given by [17]:

$$\gamma_{Bk}^0(r) = \frac{1}{1 - \left[\frac{\varphi^0(r)}{p}\right]} = \frac{1}{1 - \left[\frac{n^0(r)}{n^{\max}}\right]} = \frac{1}{1 - \left[\frac{n^0(r)V_c}{p}\right]}, \quad (3)$$

where p is the packing fraction and n^{\max} is the maximum counterion concentration for a given packing which are related by:

$$p = n^{\max}V_c. \quad (4)$$

The counterion volume fraction $\varphi^0(r)$ may also be expressed as:

$$\varphi^0(r) = p\left[\frac{n^0(r)}{n^{\max}}\right]. \quad (5)$$

Regarding the packing fraction, recall that for face-centered cubic packing, $p_{fcc} = \pi\sqrt{2}/6 = 0.74$; for simple cubic packing, $p_{sc} = \pi/6 = 0.524$; for body-centered cubic packing, $p_{bcc} = \pi\sqrt{3}/8 = 0.68$; and for random close packing, $p_{rp} = 0.64$.

The Bikerman's model is thus based on a correction to the ionic concentration in order to consider that the volume available for any ion cannot include that occupied by all other ions and their hydration layers. From his original derivation, p in Eq. (3) must simply be set equal to 1, and so the model may in principle allow a perfect packing of ions. A refinement aimed at making the model more realistic was proposed in Ref. [27] and later in Ref. [17] by introducing the packing fraction p related to the arrangement of the finite-size ions in the medium. The less-heuristic CS approach is based on a model of hard-sphere fluid, with only excluded-volume interactions between the spheres. Performing a virial expansion of the compressibility factor Z , Carnahan and Starling reached a closed form for Z that agrees very well with molecular dynamics calculations. Based on this expression for the compressibility factor, Eq. (1) is easily obtained. A systematic comparison between the different calculations of steric interactions between ions can be found in Ref. [28].

As previously mentioned, a step forward of the model is the consideration of counterions of finite size as dielectric spheres. This gives rise to the inclusion of new forces acting on the counterions (Born and dielectrophoretic forces) in addition to the electrical, thermal, and steric ones. Thus, an electrical permittivity dependence on the local counterion concentration inside the cell is assumed [19]. In what follows

we will analyze the effect of including such new counterion forces in a salt-free colloid at equilibrium.

In the liquid part of the spherical cell, from Gauss law in its differential form we have:

$$\begin{aligned} \vec{\nabla} \cdot [\varepsilon_e^0(r)\vec{\nabla}\Psi^0(r)] &= \vec{\nabla}\varepsilon_e^0(r) \cdot \vec{\nabla}\Psi^0(r) + \varepsilon_e^0(r)\nabla^2\Psi^0(r) \\ &= -zen^0(r), \end{aligned} \quad (6)$$

where $\Psi^0(r)$ denotes the equilibrium electrical potential at a radial distance r , $\varepsilon_e^0(r)$ is the effective electrical permittivity of the solution according to a Maxwell-like mixture formula [29]:

$$\frac{\varepsilon_e^0(r) - \varepsilon_s}{\varepsilon_e^0(r) + 2\varepsilon_s} = \left(\frac{\varepsilon_i - \varepsilon_s}{\varepsilon_i + 2\varepsilon_s}\right)\varphi^0(r), \quad (7)$$

from which the effective electrical permittivity is obtained as:

$$\varepsilon_e^0(r) = \varepsilon_s \left[\frac{1 + 2\Phi\varphi^0(r)}{1 - \Phi\varphi^0(r)} \right], \quad (8)$$

where

$$\Phi = \left(\frac{\varepsilon_i - \varepsilon_s}{\varepsilon_i + 2\varepsilon_s}\right), \quad (9)$$

where again $\varphi^0(r)$ is the counterion volume fraction at a radial distance r which can be related to the counterion concentration $n^0(r)$ by Eq. (2), $\varepsilon_i = \varepsilon_{ri}\varepsilon_0$ is the effective electrical permittivity of a counterion and $\varepsilon_s = \varepsilon_{rs}\varepsilon_0$ that of the continuous solution (ε_{ri} and ε_{rs} are the relative permittivities of counterions and original solution, respectively, and ε_0 is the electric permittivity of a vacuum), z is the counterion valence, and e is the elementary electric charge. From Eqs. (6)–(9), a second-order differential equation for the equilibrium electric potential $\Psi^0(r)$ can be obtained as:

$$\begin{aligned} \nabla^2\Psi^0(r) &= \frac{d^2\Psi^0(r)}{dr^2} + \frac{2}{r}\frac{d\Psi^0(r)}{dr} \\ &= -\left\{ \frac{zen^0(r)}{\varepsilon_e^0(r)} + \frac{3\Phi V_c}{[1 + \Phi n^0(r)V_c - 2\Phi^2 n^0(r)^2 V_c^2]} \right. \\ &\quad \left. \times \frac{dn^0(r)}{dr} \frac{d\Psi^0(r)}{dr} \right\}. \end{aligned} \quad (10)$$

On the other hand, the sum of the forces acting on a counterion at equilibrium, namely electric, thermal, steric, Born, and dielectrophoretic forces, vanishes [30]:

$$\begin{aligned} -ze\vec{\nabla}\Psi^0(r) - k_B T \vec{\nabla} \ln n^0(r) - k_B T \vec{\nabla} \ln \gamma^0(r) \\ - \frac{z^2 e^2}{8\pi R} \vec{\nabla} \left[\frac{1}{\varepsilon_e^0(r)} \right] + 2\pi R^3 \varepsilon_e^0(r) \frac{\varepsilon_i - \varepsilon_e^0(r)}{\varepsilon_i + 2\varepsilon_e^0(r)} \vec{\nabla} \{[-\vec{\nabla}\Psi^0(r)] \\ \cdot [-\vec{\nabla}\Psi^0(r)]\} = 0, \end{aligned} \quad (11)$$

where k_B is the Boltzmann constant and T is the absolute temperature. The last two addends of Eq. (11) stand for the Born and dielectrophoretic forces, respectively. The Born force appears when the permittivity of the solution is allowed to change with position: ions tend to move to regions of higher permittivity in order to decrease their electrostatic energy. The dielectrophoretic force appears when ions are assumed to behave as dielectric spheres, which become polarized by an external electric field acquiring an induced dipole moment.

Operating in Eq. (11), one obtains:

$$ze \frac{d\Psi^0(r)}{dr} + k_B T \frac{d \ln[\gamma^0(r)n^0(r)]}{dr} - \frac{z^2 e^2}{8\pi R \varepsilon_e^0(r)^2} \frac{d\varepsilon_e^0(r)}{dr} - \frac{4\pi R^3 \varepsilon_e^0(r)[\varepsilon_i - \varepsilon_e^0(r)]}{\varepsilon_i + 2\varepsilon_e^0(r)} \frac{d\Psi^0(r)}{dr} \frac{d^2\Psi^0(r)}{dr^2} = 0. \quad (12)$$

By using Eqs. (A2)–(A4) from the Appendix in Ref. [14], Eq. (12) becomes:

$$\frac{dn^0(r)}{dr} [1 + \Upsilon(r) + \Xi(r)] = - \frac{zen^0(r)}{k_B T} \frac{d\Psi^0(r)}{dr} \left[1 + \Sigma(r) \frac{d^2\Psi^0(r)}{dr^2} \right], \quad (13)$$

where $\Upsilon(r)$ denotes either the Carnahan-Starling approach and is defined by:

$$\Upsilon(r)_{CS} = n^0(r) \frac{d \ln \gamma^0(r)_{CS}}{dn^0(r)} = \frac{8 \varphi^0(r) - 2 \varphi^0(r)^2}{[1 - \varphi^0(r)]^4} \quad (14)$$

or by the Bikerman one defined by:

$$\Upsilon(r)_{Bk} = n^0(r) \frac{d \ln \gamma^0(r)_{Bk}}{dn^0(r)} = \frac{\left[\frac{n^0(r)}{n^{\max}} \right]}{1 - \left[\frac{n^0(r)}{n^{\max}} \right]} = \frac{\varphi^0(r)}{p \left[1 - \frac{\varphi^0(r)}{p} \right]}. \quad (15)$$

The $\Xi(r)$ and $\Sigma(r)$ functions are given by:

$$\Xi(r) = - \frac{3z^2 e^2 \Phi n^0(r) V_c}{8\pi k_B T R \varepsilon_s [1 + 2\Phi n^0(r) V_c]^2} \quad (16)$$

$$\Sigma(r) = - \frac{4\pi R^3 \varepsilon_e^0(r) [\varepsilon_i - \varepsilon_e^0(r)]}{ze [\varepsilon_i + 2\varepsilon_e^0(r)]} = - \frac{4\pi R^3 \left\{ \varepsilon_i \varepsilon_s [1 + 2\Phi n^0(r) V_c] [1 - \Phi n^0(r) V_c] - \varepsilon_s^2 [1 + 2\Phi n^0(r) V_c]^2 \right\}}{ze \left\{ \varepsilon_i [1 - \Phi n^0(r) V_c]^2 + 2\varepsilon_s [1 + 2\Phi n^0(r) V_c] [1 - \Phi n^0(r) V_c] \right\}}. \quad (17)$$

For numerical reasons it is convenient to differentiate Eq. (10) and Eq. (13) to build third- and second-order differential equations in the equilibrium electrical potential and counterion concentration, respectively, and add some extra boundary conditions. This procedure leads to the differential equations:

$$\frac{d^3\Psi^0(r)}{dr^3} = \frac{2}{r^2} \frac{d\Psi^0(r)}{dr} - \frac{2}{r} \frac{d^2\Psi^0(r)}{dr^2} - \left\{ \frac{ze}{\varepsilon_s} \frac{dn^0(r)}{dr} \left[\frac{1 - 2\Phi n^0(r) V_c - 2\Phi^2 n^0(r)^2 V_c^2}{1 + 4\Phi n^0(r) V_c + 4\Phi^2 n^0(r)^2 V_c^2} \right] + 3\Phi V_c \Pi(r) \right\}, \quad (18)$$

where the $\Pi(r)$ function is defined by:

$$\Pi(r) = \frac{\left[\frac{d^2 n^0(r)}{dr^2} \frac{d\Psi^0(r)}{dr} + \frac{dn^0(r)}{dr} \frac{d^2\Psi^0(r)}{dr^2} \right]}{\left[1 + \Phi n^0(r) V_c - 2\Phi^2 n^0(r)^2 V_c^2 \right]} - \frac{\left[\frac{dn^0(r)}{dr} \right]^2 \frac{d\Psi^0(r)}{dr} [\Phi V_c - 4\Phi^2 n^0(r) V_c^2]}{\left[1 + \Phi n^0(r) V_c - 2\Phi^2 n^0(r)^2 V_c^2 \right]^2} \quad (19)$$

and

$$\frac{d^2 n^0(r)}{dr^2} = - \frac{\frac{dn^0(r)}{dr} \left[\frac{d\Upsilon(r)}{dr} + \frac{d\Xi(r)}{dr} \right] + \frac{ze}{k_B T} \left\{ \left[\frac{dn^0(r)}{dr} \frac{d\Psi^0(r)}{dr} + n^0(r) \frac{d^2\Psi^0(r)}{dr^2} \right] [1 + \Sigma(r) \frac{d^2\Psi^0(r)}{dr^2}] + G(r) \right\}}{1 + \Upsilon(r) + \Xi(r)}, \quad (20)$$

where the $G(r)$ function is defined by:

$$G(r) = n^0(r) \frac{d\Psi^0(r)}{dr} \left[\frac{d\Sigma(r)}{dr} \frac{d^2\Psi^0(r)}{dr^2} + \Sigma(r) \frac{d^3\Psi^0(r)}{dr^3} \right]. \quad (21)$$

The corresponding boundary conditions for Eq. (18) and Eq. (20) are

$$\frac{d\Psi^0}{dr}(a) = - \frac{\sigma}{\varepsilon_e^0(a)} = - \frac{\sigma [1 - \Phi n^0(a) V_c]}{\varepsilon_s [1 + 2\Phi n^0(a) V_c]}, \quad (22)$$

$$\frac{d\Psi^0}{dr}(b) = 0, \quad (23)$$

$$\Psi^0(b) = 0, \quad (24)$$

$$n^0(b) = \frac{1}{2\Phi V_c} + \frac{\varepsilon_s}{ze} \frac{d^2\Psi^0}{dr^2}(b) + \sqrt{\left(\frac{1}{2\Phi V_c} \right)^2 + \frac{4\varepsilon_s}{ze} \frac{d^2\Psi^0}{dr^2}(b) \left(\frac{1}{2\Phi V_c} \right) + \frac{\varepsilon_s^2}{z^2 e^2} \left[\frac{d^2\Psi^0}{dr^2}(b) \right]^2}, \quad (25)$$

$$\frac{dn^0}{dr}(b) = 0, \quad (26)$$

where σ is the particle surface charge density. Equation (25) has been obtained by particularizing Eq. (10) at $r = b$ and making use of Eqs. (2) and (7). We use the mathematical application MATLAB with its built-in routine `bvp4c` to solve the differential equations with their boundary conditions. Mesh selection and error control are based on the residuals of the continuous solution. The relative tolerance, which applies to all components of the residual vector, has been taken as equal to 10^{-6} .

III. SOME NUMERICAL RESULTS AT EQUILIBRIUM

In this section we will explore the effects on the dimensionless equilibrium electric potential $e\Psi^0(r)/(k_B T)$, and the molar equilibrium counterion concentration $c^0(r) = n^0(r)/(10^3 N_A)$ (N_A is Avogadro's number) of the spatial dependence of the effective permittivity of the solution (Born and dielectrophoretic forces are included in this study). The first comparison that we will consider will be carried out between point-like, Bikerman, and Carnahan and Starling predictions, PL, Bk (the packing factor has been $p = 0.74$, corresponding to closest packing (fcc or hcp)) and C-S, respectively. Thus, in Figs. 1(a)–1(c) we show the radial dependence of the relative effective permittivity of the solution, the dimensionless equilibrium electrical potential and the molar equilibrium counterion concentration for different relative permittivities of the counterions and a particle surface charge density $\sigma = -40.0 \mu\text{C}/\text{cm}^2$. Ionic radii and effective ionic permittivity values have been taken from [31,32].

Figure 1(a) clearly shows the decrease in effective permittivity as we approach the particle surface from the solution. It is an expected feature as the counterion permittivity in this study is, in one of the cases considered, much lower ($\epsilon_{ri} = 20$) than that of the pure solution ($\epsilon_{ri} = 78.54$), and the concentration of counterions is larger near the particle surface (see Fig. 1(c) in comparison with that in the solution). This result has an important influence on the equilibrium electric potential profile in Fig. 1(b) the potential at any position increases for the lower counterion permittivity (compare with the case $\epsilon_{ri} = \epsilon_{rs}$). Despite there is not much change in the equilibrium counterion concentration upon decreasing the counterion permittivity in Fig. 1(c), the equilibrium potential is quite dependent on this quantity, and mostly for the CS approach. It is well known that a smaller permittivity in a given region in an electric field leads to an increase of the corresponding electric potential in such region. In the next section we will explore whether this effect, which involves a decreased screening of the particle charge (on top of that related to the finite size of the counterions [14]), is relevant or not for the electrokinetic properties in the present study.

IV. NONEQUILIBRIUM EFFECTS

A. New electrokinetic equations and boundary conditions

Let us again consider a spherical particle of radius a , surface charge density σ , mass density ρ_p , and relative permittivity ϵ_{rp} surrounded by a shell of a solution of effective electrical permittivity $\epsilon_e(\vec{r}, t)$ with outer radius $b = a \phi^{-1/3}$ (the radius of the cell), where ϕ is the particle volume fraction of the colloid. An alternating electric field $\vec{E} \exp(-j\omega t)$ of

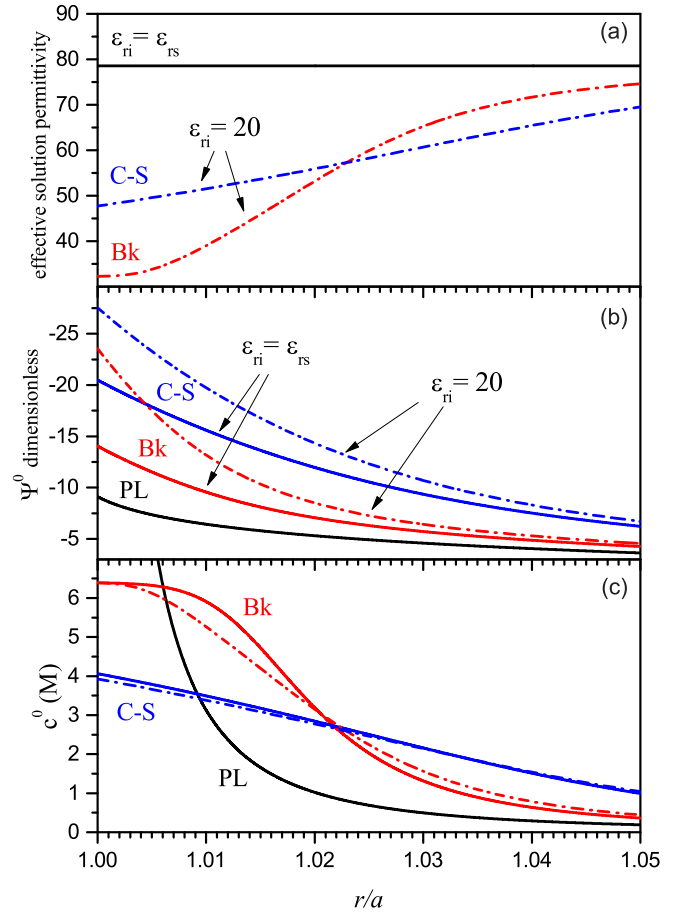


FIG. 1. (a) Relative effective permittivity of the solution, (b) Dimensionless equilibrium electrical potential, and (c) Molar equilibrium counterion concentration as a function of the dimensionless radial distance r/a from the particle center. Data according to PL, Bk (fcc packing factor) and C-S approaches for a salt-free colloid with different relative permittivities of the counterions $\epsilon_{ri} = 20$ and $\epsilon_{ri} = \epsilon_{rs} = 78.54$, with $\phi = 0.3$, $\sigma = -40.0 \mu\text{C}/\text{cm}^2$, $a = 25 \text{ nm}$ and counterion radius $R = 0.358 \text{ nm}$ (Na^+).

angular frequency ω is applied to the system. In the stationary state, the particle will move with a velocity $\vec{v}_e \exp(-j\omega t)$ where $\vec{v}_e = u_e \vec{E}$, where u_e is the dynamic electrophoretic mobility (the notation $u_{e,dc}$ will refer to the electrophoretic mobility for the dc or $\omega \rightarrow 0$ limit). A spherical coordinate system (r, θ, φ) is fixed at the center of the particle, and the polar axis ($\theta = 0$) is chosen to be parallel to the applied electric field. For the present study and according to the new features mentioned linked to the finite size, the dielectric nature of the counterions and the local dependencies with counterion concentration of the solution permittivity, the viscosity, and the counterion drag coefficient, a more complete set of electrokinetic equations, generalizing that of the standard electrokinetic model [6,7], is mandatory. The fundamental equations connecting the electrical potential $\Psi(\vec{r}, t)$, the concentration of counterions $n(\vec{r}, t)$ and their drift velocity $\vec{v}(\vec{r}, t)$, and the fluid velocity $\vec{u}(\vec{r}, t)$ and the pressure $P(\vec{r}, t)$ at every point \vec{r} in the system and time t are now

expressed as:

$$\vec{\nabla} \cdot [\varepsilon_e(\vec{r}, t) \vec{\nabla} \Psi(\vec{r}, t)] = -\rho_{\text{el}}(\vec{r}, t) = -zen(\vec{r}, t), \quad (27)$$

$$-\eta(\vec{r}, t) \vec{\nabla} \times \vec{\nabla} \times \vec{u}(\vec{r}, t) + \vec{\nabla} \eta(\vec{r}, t) \cdot [\vec{\nabla} \vec{u}(\vec{r}, t) + \vec{\nabla} \vec{u}(\vec{r}, t)^T] - \vec{\nabla} P(\vec{r}, t) - \rho_{\text{el}}(\vec{r}, t) \vec{\nabla} \Psi(\vec{r}, t) = \rho_s \frac{\partial}{\partial t} [\vec{u}(\vec{r}, t) + \vec{V}_p \exp(-i\omega t)], \quad (28)$$

$$\vec{\nabla} \cdot \vec{u}(\vec{r}, t) = 0, \quad (29)$$

$$\vec{v}(\vec{r}, t) = \vec{u}(\vec{r}, t) - \frac{1}{\lambda(\vec{r}, t)} \left\{ \vec{\nabla} \mu(\vec{r}, t) - 2\pi R^3 \varepsilon_e(\vec{r}, t) \frac{\varepsilon_i - \varepsilon_e(\vec{r}, t)}{\varepsilon_i + 2\varepsilon_e(\vec{r}, t)} \vec{\nabla} \{ [-\vec{\nabla} \Psi(\vec{r}, t)] \cdot [-\vec{\nabla} \Psi(\vec{r}, t)] \} \right\}, \quad (30)$$

$$\mu(\vec{r}, t) = \mu^\infty + ze\Psi(\vec{r}, t) + k_B T \ln[\gamma(\vec{r}, t) n(\vec{r}, t)] + \frac{z^2 e^2}{8\pi R \varepsilon_e(\vec{r}, t)}, \quad (31)$$

$$\vec{\nabla} \cdot [n(\vec{r}, t) \vec{v}(\vec{r}, t)] = -\frac{\partial n(\vec{r}, t)}{\partial t}. \quad (32)$$

Equation (27) is Poisson's equation, where $\rho_{\text{el}}(\vec{r}, t)$ is the electric charge density. Equations (28) and (29) are the Navier-Stokes equations for an incompressible fluid flow of nonhomogeneous viscosity $\eta(\vec{r}, t)$ and mass density ρ_s at low Reynolds number in the presence of an electrical body force, expressed in the present case in a more general way than those of the standard electrokinetic model (the additional term $\vec{\nabla} \eta(\vec{r}, t) \cdot [\vec{\nabla} \vec{u}(\vec{r}, t) + \vec{\nabla} \vec{u}(\vec{r}, t)^T]$, where T means a transposed tensor, has been included because of the spatial dependence of the viscosity). Note that in general, in the considered theoretical model, the density of the solution should also be a function of the ionic volume fraction. However, for mathematical simplicity, as a first approximation, the density has been assumed to be constant and equal to that of the fluid phase ρ_s . We are concerned in this work with the linear electrokinetic response of a concentrated salt-free colloid in the presence of low-strength electric fields. For that reason, the nonlinear term $-\rho(\vec{r}, t)[\vec{u}(\vec{r}, t) \cdot \vec{\nabla}] \vec{u}(\vec{r}, t)$ has been eliminated from the left-hand side of the Navier-Stokes equation (28). Equation (30) derives from the Nernst-Planck equation for the flow of the counterion species, including the gradient of its electrochemical potential $\mu(\vec{r}, t)$ defined in Eq. (31) where μ^∞ is the electrochemical potential of the counterions at a standard state, and $\lambda(\vec{r}, t) = k_B T / D_c(\vec{r}, t)$ its nonhomogeneous counterion drag coefficient. The effective electrical permittivity, the solution viscosity, and the counterion drag coefficient [or the counterion diffusion coefficient $D_c(\vec{r}, t)$] are functions of the local counterion concentration, recovering their bulk values, ε_s , η_s , and λ (or D_c), respectively, very far from the particle surface. $\gamma(\vec{r}, t)$ in Eq. (31) is the nonequilibrium activity coefficient of the counterion and it will be assumed to explicitly maintain a similar concentration dependence as either the Carnahan-Starling activity coefficient [see Eq. (1)] or the Bikerman activity coefficient [see Eq. (3)]. Finally, Eq. (32) is the

continuity equation for the conservation of the counterion species.

Summarizing, some of the standard electrokinetic equations have been changed to account for the new features linked to the dielectric nature of the counterions that lead to a permittivity dependence with the local counterion concentration in solution and new related forces acting on the counterions. In addition, it has also been considered that the viscosity of the solution, as well as the counterion diffusion coefficient, may be nonhomogeneous, recovering their bulk values in the solution far from the charged particle surface. We will follow the original work of López-García *et al.* [19] where all these aspects have been addressed for dilute colloids in general electrolyte solutions under the Smoluchowski approximation, but with the appropriate modifications pertaining to the case of concentrated salt-free colloids. As referred to above, one of the main aspects implemented in the present approach refers to the substitution of the Batchelor-Green equation [22] used by the latter authors by our RR&C model [23], which has proved successful in explaining some viscosity experiments with silica colloids [33] by using effective particle volume fractions. In terms of the equilibrium counterion volume fraction $\varphi^0(r)$, or its related counterion concentration $n^0(r)$ [see Eq. (2)], the local viscosity of the nonhomogeneous solution according to the RR&C model can be expressed as:

$$\eta^0(r) = \eta_s \left[1 + \frac{5}{2} \varphi^0(r) S^0(r) \right] = \eta_s \left[1 + \frac{5}{2} n^0(r) V_c S^0(r) \right] \quad (33)$$

in the absence of external electric fields, where η_s corresponds to the viscosity of the pure solution and $S^0(r)$ is an adaptation for the present case of a particularization of the original Simha function [24] already used by the authors [23] including a condition on the size of the cell due to Happel [25]. Such adaptation (denominated RR&C or modified Simha) is given by:

$$S^0(r) = \frac{4[1 - \varphi^0(r)^{7/3}]}{4[1 + \varphi^0(r)^{10/3}] - 25 \varphi^0(r)[1 + \varphi^0(r)^{4/3}] + 42 \varphi^0(r)^{5/3}}. \quad (34)$$

Admitting the proportionality between the drag coefficient of counterions and the local viscosity, it can be proposed that the ratio between $\lambda^0(r)$ (equilibrium drag coefficient at any position) and λ (equilibrium drag coefficient in the bulk) coincides with the ratio between the corresponding viscosities, as follows:

$$\lambda^0(r) = \frac{\lambda}{\eta_s} \eta^0(r) = \lambda \left[1 + \frac{5}{2} n^0(r) V_c \mathcal{S}^0(r) \right]. \quad (35)$$

For very low counterion concentrations ($\varphi^0 \rightarrow 0$) the \mathcal{S}^0 function tends to unity and the Einstein equation for the viscosity of a dilute suspension of hard spheres is recovered. If the effect on the solution viscosity of the local counterion concentration is neglected, then the constant values η_s and λ for the bulk solution viscosity and counterion drag coefficient can be used whatever the point in the solution. In Fig. 2 it is shown a comparison between the viscosity of a system of hard spherical particles as a function of particle volume fraction φ^0 according to Batchelor-Green [22], Eilers [34], Mooney [35], and the RR&C (modified Simha) hard-sphere models [23]. All of them converge to the Einstein model [36] (also displayed in Fig. 2) as the volume fraction tends to zero. The most significant feature for the present work in Fig. 2 is the notable increase in relative viscosity with counterion volume fraction predicted by the RR&C model when compared to the predictions of the rest of the models. Recall that a previous study [19], which used the Batchelor-Green viscosity model, concluded that it certainly underestimated the solution viscosity at high volume fractions (like those taking place in our condensate counterion region). For this reason and according to the above-mentioned successful explanation of recent viscosity data of silica colloids with the RR&C model [33], this will be used in the solution of the general problem.

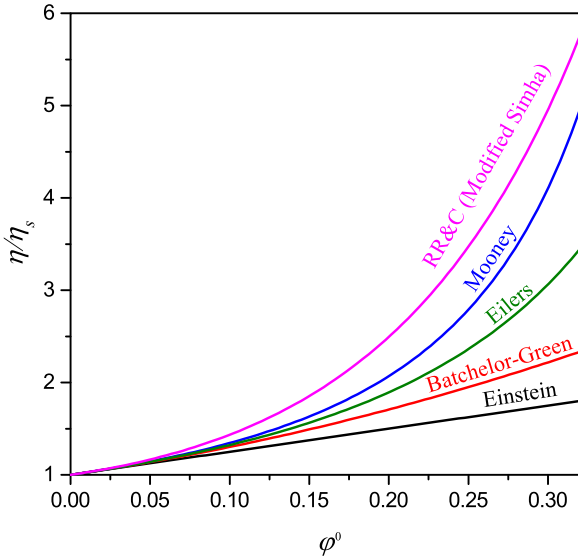


FIG. 2. Comparison between the relative viscosity predictions for a system of spherical particles as a function of hard-sphere volume fraction according to Einstein, Batchelor-Green, Eilers, and Mooney for random close packing and RR&C (modified Simha) hard-sphere models.

As we are interested in the linear response to low-strength electric fields, a first-order perturbation procedure can be applied. This has been commonly used in the literature [37,38] but it has to be extended to include a similar scheme for the Carnahan-Starling or Bikerman activity coefficients $\gamma(\vec{r}, t)$, the effective electrical permittivity $\varepsilon_e(\vec{r}, t)$, the solution viscosity $\eta(\vec{r}, t)$, and the drag counterion coefficient $\lambda(\vec{r}, t)$ [related to the counterion diffusion coefficient $D_c(\vec{r}, t)$ by $D_c(\vec{r}, t) = k_B T / \lambda(\vec{r}, t)$] in the presence of an alternating electric field $\vec{E} \exp(-j\omega t)$. To that aim, the quantities of interest, $X(\vec{r}, t)$, say, are expressed as the sum of an equilibrium term $X^0(r)$ plus a perturbation linearly dependent of the field $\delta X(\vec{r}) \exp(-j\omega t)$. Note that the equilibrium term is zero in the case of both the counterion and fluid velocities [$\vec{u}(\vec{r}, t) = \delta \vec{u}(\vec{r}) \exp(-j\omega t)$, $\vec{v}(\vec{r}, t) = \delta \vec{v}(\vec{r}) \exp(-j\omega t)$].

The symmetry of the problem permits us to express the linear perturbations [37]:

$$\delta \vec{u}(\vec{r}) = \left[-\frac{2h}{r} E \cos \theta, \frac{1}{r} \frac{d(rh)}{dr} E \sin \theta, 0 \right], \quad (36)$$

$$\delta \mu(\vec{r}) = -ze\phi(r)E \cos \theta, \quad (37)$$

$$\delta \Psi(\vec{r}) = -Y(r)E \cos \theta, \quad (38)$$

$$\delta \Psi_p(\vec{r}) = -Y_p(r)E \cos \theta, \quad (39)$$

$$\delta P(\vec{r}) = \chi(r)E \cos \theta, \quad (40)$$

$$\begin{aligned} \delta n(\vec{r}) &= \frac{n^0(r) S(r)}{k_B T} [\delta \mu(\vec{r}) - ze\delta \Psi(\vec{r})] \\ &= -\frac{zen^0(r) S(r)}{k_B T} [\phi(r) - Y(r)]E \cos \theta, \end{aligned} \quad (41)$$

$$\delta \varepsilon_e(\vec{r}) = \frac{3\varepsilon_{rs}\varepsilon_0\Phi V_c}{[1 - \Phi n^0(r)V_c]^2} \delta n(\vec{r}), \quad (42)$$

$$\delta \eta(\vec{r}) = \frac{5}{2} \eta_s [n^0(r) \mathcal{Q}(r) + \mathcal{S}^0(r)] V_c \delta n(\vec{r}), \quad (43)$$

$$\delta \lambda(\vec{r}) = \frac{5}{2} \lambda [n^0(r) \mathcal{Q}(r) + \mathcal{S}^0(r)] V_c \delta n(\vec{r}), \quad (44)$$

in terms of some radial functions $h(r)$, $Y(r)$, $Y_p(r)$, $\chi(r)$, and $\phi(r)$, which contain information about the field-induced linear perturbations (the subscript p denotes the solid particle). To better understand the previous and subsequent equations, the reader is referred to Appendix A, where expressions for the functions $S(r)$ and $\mathcal{Q}(r)$ can also be found.

As the nonhomogeneous drag counterion coefficient $\lambda(\vec{r}, t)$ is also assumed to be related to the nonhomogeneous solution viscosity in an analogous form to that in homogeneous solutions, one can write:

$$\begin{aligned} \lambda(\vec{r}, t) &= \frac{\lambda}{\eta_s} \eta(\vec{r}, t) = \lambda^0(r) + \delta \lambda(\vec{r}) \exp(-j\omega t) \\ &= \frac{\lambda}{\eta_s} [\eta^0(r) + \delta \eta(\vec{r}) \exp(-j\omega t)] \end{aligned} \quad (45)$$

and by simply using Eq. (43), Eq. (44) is finally obtained.

The new linearized Navier-Stokes equation turns out to be

$$\begin{aligned} \mathcal{L}^2 h(r) + \frac{j\omega\rho_s}{\eta^0(r)} \mathcal{L}h(r) + \frac{1}{\eta^0(r)} \left[\frac{d\eta^0(r)}{dr} \right] \left[2 \frac{d^3 h(r)}{dr^3} + \frac{4}{r} \frac{d^2 h(r)}{dr^2} - \frac{6}{r^2} \frac{dh(r)}{dr} + \frac{6}{r^3} h(r) \right] + \frac{1}{\eta^0(r)} \frac{d^2 \eta^0(r)}{dr^2} \frac{d^2 h(r)}{dr^2} \\ = - \frac{z^2 e^2 n^0(r)}{k_B T \eta^0(r) r} \left[\frac{d\Psi^0(r)}{dr} \right] S(r) \left[\phi(r) + Y(r) \Sigma(r) \frac{d^2 \Psi^0(r)}{dr^2} \right], \end{aligned} \quad (46)$$

where the $\Sigma(r)$ function was defined in Eq. (17) and the operators \mathcal{L} and \mathcal{L}^2 are

$$\mathcal{L} \equiv \frac{d^2}{dr^2} + \frac{2}{r} \frac{d}{dr} - \frac{2}{r^2}, \quad (47)$$

$$\mathcal{L}^2 \equiv \frac{d^4}{dr^4} + \frac{4}{r} \frac{d^3}{dr^3} - \frac{4}{r^2} \frac{d^2}{dr^2}. \quad (48)$$

The linearized continuity equation for the general case is

$$\begin{aligned} \mathbb{J}(r) + n^0(r) \left\{ \frac{ze}{\lambda^0(r)} \mathcal{L}\phi(r) + \frac{\lambda}{\lambda^0(r)} \left[r^2 \frac{df(r)}{dr} + 4rf(r) + \frac{dy(r)}{dr} + r^2 \frac{d\zeta(r)}{dr} + 4r\zeta(r) \right] \right. \\ \left. - \frac{\lambda}{\lambda^0(r)^2} \frac{d\lambda^0(r)}{dr} \left[r^2 f(r) + y(r) + r^2 \zeta(r) + \frac{ze}{\lambda} \frac{d\phi(r)}{dr} \right] \right\} \\ = - \frac{j\omega ze n^0(r) S(r)}{k_B T} [\phi(r) - Y(r)], \end{aligned} \quad (49)$$

where the auxiliary $\mathbb{J}(r)$, $f(r)$, $y(r)$, and $\zeta(r)$ functions are detailed in Appendix A. Finally, the third-order version of the linearized, modified Poisson equation reads

$$\begin{aligned} \frac{d^3 Y(r)}{dr^3} + \frac{2}{r} \frac{d^2 Y(r)}{dr^2} - \frac{4}{r^2} \frac{dY(r)}{dr} + \frac{4}{r^3} Y(r) \\ = A(r) + B(r) + C(r) + D(r) \end{aligned} \quad (50)$$

and the functions $A(r)$, $B(r)$, $C(r)$, $D(r)$ can also be found in Appendix A.

The appropriate boundary conditions for the latter system of electrokinetic equations are [7,39]:

$$\Psi_p(\vec{r}, t) = \Psi(\vec{r}, t) \quad \text{at } r = a, \quad (51)$$

$$\varepsilon_{rs} \vec{\nabla} \Psi(\vec{r}, t) \cdot \hat{r} - \varepsilon_{rp} \vec{\nabla} \Psi_p(\vec{r}, t) \cdot \hat{r} = -\sigma/\varepsilon_0 \quad \text{at } r = a, \quad (52)$$

$$\vec{u}(\vec{r}, t) = 0 \quad \text{at } r = a, \quad (53)$$

$$\vec{\nabla}(\vec{r}, t) \cdot \hat{r} = 0 \quad \text{at } r = a, \quad (54)$$

$$\vec{\omega}(\vec{r}, t) = \vec{\nabla} \times \vec{u}(\vec{r}, t) = 0 \quad \text{at } r = b, \quad (55)$$

$$n(\vec{r}, t) - n^0(r) = 0 \quad \text{at } r = b, \quad (56)$$

$$\Psi(\vec{r}, t) - \Psi^0(r) = -\vec{E} \cdot \vec{r} \exp(-j\omega t) \quad \text{at } r = b. \quad (57)$$

In addition, an integral condition is chosen for obtaining the electrophoretic mobility:

$$\langle \rho_m \vec{u}'(\vec{r}, t) \rangle = \frac{1}{V_{\text{cell}}} \int_{V_{\text{cell}}} \rho_m \vec{u}'(\vec{r}, t) dV = 0, \quad (58)$$

where $\vec{u}'(\vec{r}, t)$ is the local velocity with respect to a laboratory reference system, ρ_m is the local mass density, and V_{cell} the volume of the unit cell.

In summary, the boundary conditions imposed at the particle surface are expressed by Eq. (51), which denotes the continuity of the electric potential, and $\Psi_p(\vec{r}, t)$ is the potential inside the particle; Eq. (52), which represents the discontinuity of the normal component of the displacement vector (\hat{r} is the radial unit vector of the spherical coordinate system); Eq. (53), which indicates that the fluid is at rest at the particle surface in the reference system fixed to the particle; and Eq. (54), which denotes the impossibility of counterions to penetrate the solid particle. In addition, at the outer surface of the cell the chosen boundary conditions are given by Eq. (55), which corresponds to the Kuwabara boundary condition of null vorticity $\vec{\omega}$ for the fluid velocity; Eqs. (56) and (57), which are the Shilov-Zharkikh-Borkovskaya boundary conditions [40] for the perturbed concentration of counterions and perturbed electric potential in such a surface; and the integral condition in Eq. (58), which, according to O'Brien [41], imposes that the macroscopic momentum per unit volume of the colloid is zero, allowing us to obtain the dynamic electrophoretic mobility. Finally, the equation of motion of the unit cell with the net force acting on it will permit us to close the problem [37,42].

The linearized version of the boundary conditions for the general case described in Eqs. (51) and (57) can finally be expressed as:

$$h(a) = 0, \quad (59)$$

$$\frac{dh}{dr}(a) = 0, \quad (60)$$

$$\frac{d^2h}{dr^2}(b) + \frac{2}{b} \frac{dh}{dr}(b) - \frac{2}{b^2} h(b) = 0, \quad (61)$$

$$\frac{d^3h}{dr^3}(b) + \frac{1}{b} \frac{d^2h}{dr^2}(b) - \frac{6}{b^2} \frac{dh}{dr}(b) + \frac{6}{b^3} h(b) - \frac{j\omega\rho_s}{\eta^0(b)} \left[\frac{h(b)}{b} - u_e \frac{(\rho_p - \rho_s)}{\rho_s} \phi - \frac{dh}{dr}(b) \right] + \frac{1}{\eta^0(b)} \frac{d\eta^0}{dr}(b) \frac{d^2h}{dr^2}(b) = \frac{\rho_{el}^0(b) Y(b)}{b\eta^0(b)}, \quad (62)$$

$$ze \frac{d\phi}{dr}(a) - 3V_c \varepsilon_e^0(a) \frac{\varepsilon_i - \varepsilon_e^0(a)}{\varepsilon_i + 2\varepsilon_e^0(a)} \left[\frac{d^2\Psi^0}{dr^2}(a) \frac{dY}{dr}(a) + \frac{d\Psi^0}{dr}(a) \frac{d^2Y}{dr^2}(a) \right] - 9V_c^2 \frac{d\Psi^0}{dr}(a) \frac{d^2\Psi^0}{dr^2}(a) \frac{\varepsilon_i^2 - 2\varepsilon_i \varepsilon_e^0(a) - 2\varepsilon_e^0(a)^2}{[\varepsilon_i + 2\varepsilon_e^0(a)]^2} \frac{\varepsilon_{rs}\varepsilon_0 \Phi ze n^0(a) S(a) [\phi(a) - Y(a)]}{k_B T [1 - \Phi n^0(a) V_c]^2} = 0, \quad (63)$$

$$\phi(b) = b, \quad (64)$$

$$\frac{dY}{dr}(a) + 3 \frac{d\Psi^0}{dr}(a) \frac{\varepsilon_{rs}\varepsilon_0 \Phi ze V_c n^0(a) S(a) [\phi(a) - Y(a)]}{\varepsilon_e^0(a) k_B T [1 - \Phi n^0(a) V_c]^2} - \frac{\varepsilon_{rp}\varepsilon_0 Y(a)}{\varepsilon_e^0(a) a} = 0, \quad (65)$$

$$Y(b) = b, \quad (66)$$

where Eq. (62) stems from the new net force acting on the unit cell. Also, the integral condition expressed by Eq. (58) allows us to obtain the electrophoretic mobility as:

$$u_e = \frac{2h(b)}{b} \frac{1}{\left[1 + \left(\frac{\rho_p - \rho_s}{\rho_s}\right)\phi\right]}. \quad (67)$$

Regarding the derivation of the boundary condition expressed by Eq. (62), the reader is referred to Appendix A.

B. Calculation of the complex electrical conductivity and relative permittivity

As is well known in the literature concerning the electrokinetic cell model [40], the complex conductivity K^* of the colloid can be calculated from the linear relation between macroscopic electric current density $\langle \vec{i}(\vec{r}, t) \rangle$ and macroscopic electric field $\langle -\vec{\nabla}\Psi(\vec{r}, t) \rangle$. Such macroscopic quantities are expressed by volume averages of the corresponding local properties in the volume of a cell V_{cell} (S_b denotes the outer surface of the cell):

$$\langle \vec{i}(\vec{r}, t) \rangle = \frac{1}{V_{\text{cell}}} \int_{V_{\text{cell}}} \vec{i}(\vec{r}, t) dV = \frac{1}{V_{\text{cell}}} \oint_{S_b} \vec{r} \vec{i}(\vec{r}, t) \cdot \hat{r} dS_b = K^* \frac{1}{V_{\text{cell}}} \int_{V_{\text{cell}}} [-\vec{\nabla}\Psi(\vec{r}, t)] dV = K^* \langle -\vec{\nabla}\Psi(\vec{r}, t) \rangle, \quad (68)$$

where the local electric current density $\vec{i}(\vec{r}, t)$ is defined by:

$$\vec{i}(\vec{r}, t) = \rho_{el}(\vec{r}, t) \vec{v}(\vec{r}, t) + \frac{\partial \vec{D}}{\partial t} = \rho_{el}(\vec{r}, t) \vec{v}(\vec{r}, t) - \frac{\partial}{\partial t} [\varepsilon_e(\vec{r}, t) \vec{\nabla}\Psi(\vec{r}, t)]. \quad (69)$$

The macroscopic electric field must equal the volume average of the local electric field in the unit cell. In the presence of an alternating electric field $\vec{E} \exp(-j\omega t)$ and taking the perturbation procedure mentioned in Sec. V A into account, we have:

$$\begin{aligned} \langle -\vec{\nabla}\Psi(\vec{r}, t) \rangle &= \frac{1}{V_{\text{cell}}} \int_{V_{\text{cell}}} [-\vec{\nabla}\Psi^0(r) - \vec{\nabla}\delta\Psi(\vec{r})e^{-j\omega t}] dV = \frac{1}{V_{\text{cell}}} \int_{V_{\text{cell}}} [-\vec{\nabla}\delta\Psi(\vec{r})e^{-j\omega t}] dV = -\frac{1}{V_{\text{cell}}} \oint_{S_b} \delta\Psi(\vec{r})e^{-j\omega t} \hat{r} dS_b \\ &= -\frac{1}{V_{\text{cell}}} \oint_{S_b} [-Y(r)E \cos\theta] e^{-j\omega t} \hat{r} dS_b = \frac{1}{V_{\text{cell}}} Y(b)e^{-j\omega t} \oint_{S_b} E \cos\theta \hat{r} dS_b = \frac{Y(b)}{b} \vec{E} e^{-j\omega t}. \end{aligned} \quad (70)$$

It has to be pointed out that in deriving the latter equation we have used the fact that

$$\frac{1}{V_{\text{cell}}} \int_{V_{\text{cell}}} [-\vec{\nabla}\Psi^0(r)] dV = 0, \quad (71)$$

due to the spherical symmetry of the equilibrium problem. Similarly and with the help of the aforementioned linear perturbation procedure, the volume average of the local current density is calculated as (details in Appendix B):

$$\begin{aligned} \vec{i}(\vec{r}, t) &= \left\{ \frac{z^2 e^2 n^0(b)}{\lambda^0(b)} \frac{d\phi}{dr}(b) - z e n^0(b) \frac{2h(b)}{b} - j \omega \varepsilon_e^0(b) \frac{dY}{dr}(b) - 2ze \frac{2\pi R^3}{\lambda^0(b)} n^0(b) \varepsilon_e^0(b) \left[\frac{\varepsilon_i - \varepsilon_e^0(b)}{\varepsilon_i + 2\varepsilon_e^0(b)} \right] \frac{d^2 \Psi^0}{dr^2}(b) \frac{dY}{dr}(b) \right\} \\ \vec{E} e^{-j\omega t} &= K^*(\omega) (-\vec{\nabla} \Psi(\vec{r}, t)). \end{aligned} \quad (72)$$

According to Eq. (70), the complex electrical conductivity $K^*(\omega)$ can finally be obtained as:

$$K^*(\omega) = \left\{ \frac{z^2 e^2 n^0(b)}{\lambda^0(b)} \frac{d\phi}{dr}(b) - z e n^0(b) \frac{2h(b)}{b} - j \omega \varepsilon_e^0(b) \frac{dY}{dr}(b) - \frac{4ze\pi R^3}{\lambda^0(b)} n^0(b) \varepsilon_e^0(b) \left[\frac{\varepsilon_i - \varepsilon_e^0(b)}{\varepsilon_i + 2\varepsilon_e^0(b)} \right] \frac{d^2 \Psi^0}{dr^2}(b) \frac{dY}{dr}(b) \right\} \frac{b}{Y(b)}. \quad (73)$$

In the limit when Φ tends to zero [see Eq. (9)], the latter $\varepsilon_e^0(b)$ reaches the permittivity of the continuous solution $\varepsilon_{rs}\varepsilon_0$ and also $\varepsilon_i = \varepsilon_{rs}\varepsilon_0$. Likewise, if the viscosity were homogeneous, then the counterion drag coefficient would not be a function of the local counterion concentration, reaching the constant value λ , and thus Eq. (73) transforms into a simpler one already derived in a previous work where all these aspects were neglected (Eq. (61) in Ref. [14]), as counterions in such limits are not allowed to behave as polarizable dielectric spheres and have also a constant drag coefficient value.

The complex relative permittivity $\varepsilon_r^*(\omega)$ of the colloid is usually defined from the complex conductivity by the equation:

$$K^*(\omega) = K_{dc} - j\omega\varepsilon_0\varepsilon_r^*(\omega) = K_{dc} - j\omega\varepsilon_0[\varepsilon_r'(\omega) + j\varepsilon_r''(\omega)], \quad (74)$$

where $K_{dc} = K^*(\omega = 0)$. Separating real and imaginary parts we finally obtain:

$$\varepsilon_r'(\omega) = -\frac{\text{Im}[K^*(\omega)]}{\omega\varepsilon_0}, \quad (75)$$

$$\varepsilon_r''(\omega) = \frac{\text{Re}[K^*(\omega)] - K_{dc}}{\omega\varepsilon_0}. \quad (76)$$

V. SOME NUMERICAL RESULTS REGARDING THE DC AND AC MOBILITY AND DIELECTRIC DISPERSION

A. DC results

In Fig. 3(a) we study the counterion size effect according to pointlike (PL), Bikerman (Bk, fcc packing fraction), and Carnahan and Starling (C-S) approaches including additional Born and dielectrophoretic effects (BKBD and CSBD studies), and additional nonhomogeneous viscosity and counterion diffusion coefficient (BKBDVD and CSBDVD studies) on the dc electrophoretic mobility u_{edc} of a spherical particle in a concentrated salt-free colloid, expressed by its dimensionless electrophoretic mobility as:

$$u_{edc \text{ dim}} = \frac{3\eta_s e}{2\varepsilon_{rs}\varepsilon_0 k_B T} u_{edc} \quad (77)$$

and in Fig. 3(b) an analogous study on the electrical conductivity K_{dc} as a function of the particle surface charge density for Na^+ as counterion with radius $R = 0.358$ nm, $a = 25$ nm, and $\phi = 0.3$.

In Fig. 3(a) the electrophoretic mobility-charge density plot clearly shows the previously mentioned counterion

condensation effect. As it is already known, in salt-free colloids and due to the formation of a layer of counterions onto the particle surface (the ionic condensation effect), once the surface charge density reaches a characteristic value for the condensation [3,5,43], the mobility stops its increasing behavior and even decreases when the charge density is further increased. This effect is present no matter the finite-size approach used and also when the ions are considered pointlike (PL case). In a previous work addressing the effect of the finite size of counterions on the electrophoretic mobility [14], it was proposed that the lower screening of the particle charge when the counterions are allowed to have finite size was in part responsible of the larger mobility values over the PL results, much more notorious for the C-S case, as the main region of

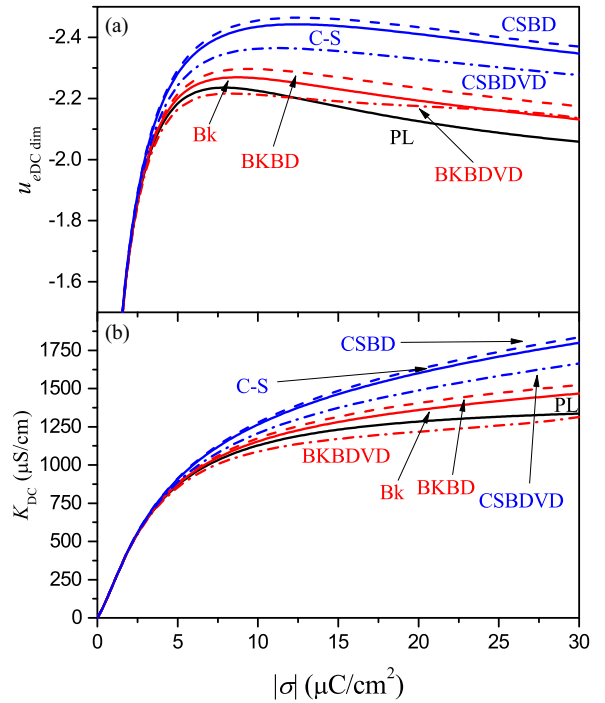


FIG. 3. (a) Dimensionless dc electrophoretic mobility and (b) dc electrical conductivity as a function of particle surface charge density for a salt-free colloid according to PL, Bk ($p = 0.74$, face-centered cubic packing) (BKBD and BKBDVD), and C-S (CSBD and CSBDVD) approaches with $R = 0.358$ nm (Na^+), $a = 25$ nm, $\phi = 0.3$, and $\varepsilon_{ri} = 20$.

the counterion excess for the latter is shifted to farther distances from the particle surface than in the other cases. It was concluded that the global effect was a reduction of the braking effect on the particle motion, forcing the electrophoretic mobility to increase at high particle surface charges [44,45]. Now when Born and dielectrophoretic effects are included [BKBD and CSBD cases, dashed lines in Fig. 3(a)], the mobility shows an additional increase over the latter results, being always larger for the Carnahan and Starling study. But what is more remarkable is the effect when both the nonhomogeneous viscosity and the nonhomogeneous counterion diffusion coefficient are taken into account (BKBDVD and CSBDVD cases, dashed-dotted lines). The above-mentioned rise of the mobility is clearly reduced in the general case in which all these effects have been considered in the theory. This effect on the mobility was also predicted for dilute colloids with thin double layers in general electrolyte solutions [19] using the Batchelor-Green viscosity model: the increase of the local viscosity of the fluid with the local concentration of counterions alters the magnitude of the counterion fluxes and fluid motion with respect to the particle, with the expected consequence of a diminution of the particle mobility. The CSBDVD case shows that the reduction in mobility with respect to the CS and CSBD predictions is not enough for the mobility to stop being greater than the standard PL prediction.

Results corresponding to the dc conductivity are displayed in Fig. 3(b). For low surface charge density, the conductivity increases linearly with the charge, as expected considering the effects of the released counterions and the particles themselves. As the surface charge is increased, the counterion condensate becomes prominent [2–4], and the conductivity does not increase further with σ , as additional ions go to mainly feed the condensate and do not participate in the charge transport, since the diffuse layer remains essentially unchanged according to the PL model. When counterion size is taken into consideration (Bk and C-S) some increase is still observed, due to the fact that ions are spread over a larger volume of the double layer, and they cannot efficiently accumulate in the condensate. Born and dielectrophoretic forces (BKBD and CSBD) have a minor effect, due to the almost cancellation of Born and dielectrophoretic forces (tending to send ions to regions far from the interface) and permittivity decrease close to the particle (tending to accumulate ions at the interface, see Ref. [30]), while adding viscosity effects (BKBDVD and CSBDVD) tends to clearly diminish the conductivity, a result associated to the decrease of the diffusion coefficient of counterions.

In addition, in Figs. 4(a) and 4(b) we show similar studies as a function of the particle volume fraction with fixed $\sigma = -40.0 \mu\text{C}/\text{cm}^2$. In Fig. 4(a) it can be appreciated that one of the most remarkable effects of accounting for ion size on the electrophoretic mobility is its increase with particle concentration in the high-concentration region according to both Bk and C-S models. This unexpected result was already studied in a previous work [14] and explained on the basis of the fact that the region of the cell in which finite-size ions are spread is wider in the Bk and C-S models. As a consequence, electro-osmotic fluxes should be enhanced and so will the electrophoretic mobility. Thus, it might be possible to overcome the braking effect on particle motion for the highest

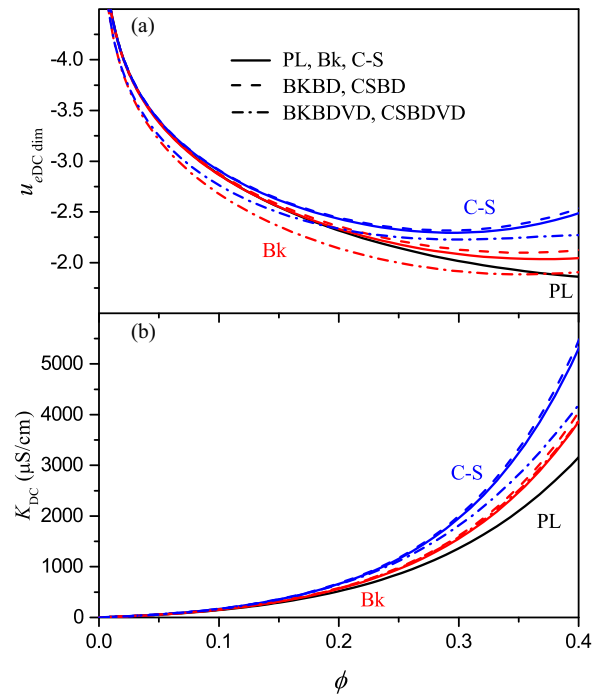


FIG. 4. (a) Dimensionless dc electrophoretic mobility and (b) dc electrical conductivity as a function of particle volume fraction for a salt-free colloid according to PL, Bk ($p = 0.74$, face-centered cubic packing) (BKBD and BKBDVD), and C-S (CSBD and CSBDVD) approaches with $R = 0.358 \text{ nm}$ (Na^+), $a = 25 \text{ nm}$, $\sigma = -40.0 \mu\text{C}/\text{cm}^2$, and $\epsilon_{ri} = 20$.

particle concentrations [44]. But according to the complete CSBDVD and BKBDVD models, this rather unrealistic effect is no longer maintained. The nonhomogeneous viscosity and counterion diffusion coefficient, both dependent on the local counterion concentration, are responsible for the neutralization of the latter enhancement.

Regarding the effects of the finite counterion size on the dependence of the dc electrical conductivity with particle concentration shown in Fig. 4(b), an overall increasing trend of the conductivity for all finite-size models is predicted, as it is more important for the C-S conditions. In general, local electric conduction is favored because of the enhancement of the concentration of the finite-size mobile counterions in liquid regions not so close to the particle surface. Also, the smaller restriction for counterion movement far from the particles allows for the increase of the overall electric current. As in the case of the electrophoretic mobility, the conductivity is essentially unaffected when Born and dielectrophoretic effects are theoretically included (BKBD and CSBD). But it is the CSBDVD case that predicts a clear diminution of the conductivity in comparison with its less-sophisticated versions (C-S and CSBD). The BKBDVD displays no clear changes with regards to its simpler finite-size versions. It is reasonable to think that the increased population of counterions far from the particle surfaces for the Carnahan-Starling approach in comparison with the other ones, as well as the negative effect of the nonhomogeneous viscosity on the counterion fluxes, are responsible for the observed smaller conductivity values for the latter conditions.

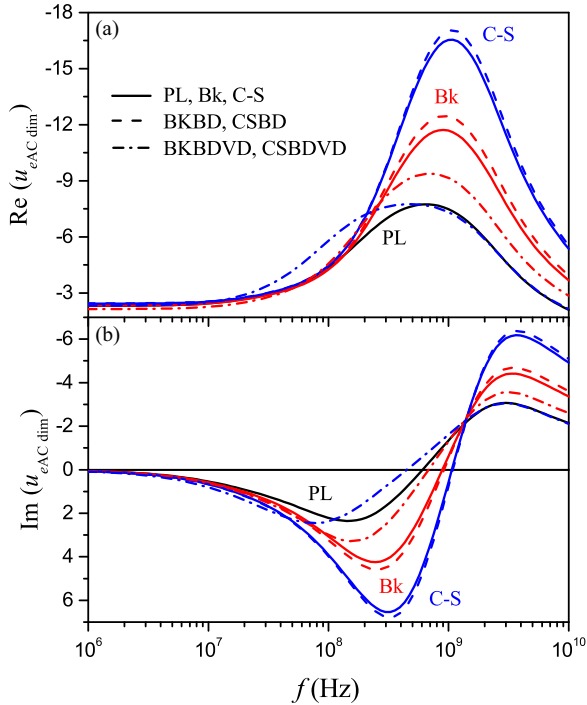


FIG. 5. Real (a) and imaginary (b) parts of the dynamic electrophoretic mobility as a function of frequency for a salt-free colloid according to PL, Bikerman (Bk, BKBD, and BKBDVD, $p = 0.74$, face-centered cubic packing), and Carnahan and Starling (C-S, CSBD, and CSBDVD) approaches with $R = 0.358$ nm (Na^+), $a = 25$ nm, $\sigma = -40.0$ $\mu\text{C}/\text{cm}^2$, $\phi = 0.2$, and $\epsilon_{ri} = 20$.

B. AC results

Figures 5(a) and 5(b) show the real and imaginary parts of the dimensionless dynamic electrophoretic mobility $u_{eac\ dim}$ [same scaling factor as that in Eq. (77)], and Figs. 6(a) and 6(b) show the real and imaginary parts of the complex relative electric permittivity ϵ_r^* , respectively, as a function of frequency for a salt-free colloid according to PL, Bikerman (Bk, BKBD, and BKBDVD, $p = 0.74$, face-centered cubic packing), and Carnahan and Starling (C-S, CSBD, and CSBDVD) approaches with $R = 0.358$ nm (Na^+), $a = 25$ nm, $\sigma = -40.0$ $\mu\text{C}/\text{cm}^2$, and $\phi = 0.2$.

As regards Fig. 5(a), the most striking feature observed is the enormous increase of the real part of the mobility at frequencies around 10^9 Hz, followed by the decrease associated to inertia. The maximum of the mobility as frequency increases is linked to the relaxation of two polarization processes, very close in frequency in the case analyzed in Fig. 5, the already known Maxwell-Wagner-O’Konski (MWO) polarization of the electric double layer [7] and the Maxwell-Wagner polarization of the counterion condensation layer (MWC) that relaxes at higher frequency than the latter because of the smaller length of the condensation layer in comparison with that of the double layer. These phenomena have been extensively studied in the recent past [14,44] and motivated an important debate because of the huge increase of the mobility maximum over its standard PL prediction. In the present case, Born and dielectrophoretic effects even increase

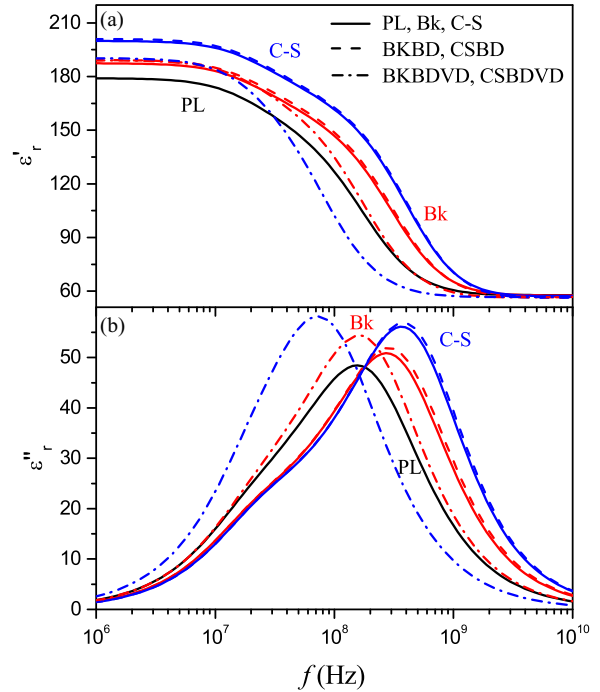


FIG. 6. Same as Fig. 5 for the real (a) and imaginary (b) parts of the complex relative permittivity.

a bit more the mobility displayed for the Bk and C-S cases [2,3,44].

However, the important feature now is the diminution of the mobility maximum when the dependence of the viscosity and diffusion counterion coefficient with the local counterion concentration are taken into account for both Bikerman and Carnahan and Starling approaches. The CSBDVD prediction is nearly coincident with the PL one past the maximum in the inertia region, dramatically reducing previous finite-size predictions for constant solution viscosity and counterion diffusion coefficient [14]. In our opinion the enhancement of the mobility maximum in frequency on relaxing the relaxation polarization processes (from around -7 to -17 for the C-S case) was a clear overestimation of the simpler models. It is unquestionable that these models lack a rigorous consideration of viscosity effects. Of course, the new predictions depend on the used model of viscosity, but the general effect seems to be that the maximum mobility decreases if a non-homogeneous solution viscosity and its effect on counterion diffusion coefficient are allowed. The effects described are less notorious for the BKBDVD case but follow a similar trend. Finally another important aspect is the frequency shift of the mobility global Maxwell-Wagner relaxation frequency for the CSBDVD case to lower frequencies in comparison with those of simpler CS and CSBD models. This fact is more clearly seen in Fig. 5(b) for the imaginary part of the dynamic mobility, as it corresponds to the first maximum [first frequency minimum in Fig. 5(b) as the y axis is inverted]. In this useful representation, the highest frequency peak corresponds to the inertial relaxation frequency of particle motion (inflection point in the real part of the mobility-frequency curve in such inertia region).

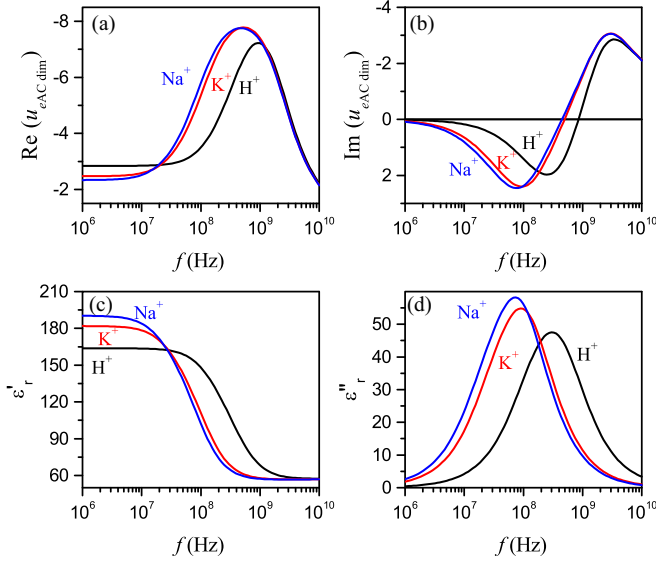


FIG. 7. Real (a) and imaginary (b) parts of the dimensionless dynamic electrophoretic mobility and real (c) and imaginary (d) parts of the complex relative permittivity as a function of frequency for a salt-free colloid according to the CSBDVD approach for three different counterions with $a = 25$ nm, $\sigma = -40.0 \mu\text{C}/\text{cm}^2$, $\phi = 0.2$, and $\epsilon_{ri} = 20$.

The real part of the complex relative electric permittivity versus frequency is displayed in Fig. 6(a). It can be observed that the permittivity increases when finite ion sizes are considered (as described in Ref. [14]). As before, Born and dielectrophoretic effects do not seem to have any influence on permittivity different from that for Bk or C-S. In Fig. 6(a) we can clearly observe the presence of the two Maxwell-Wagner relaxations, MWO and MWC. See also the presence of a shoulder in Fig. 6(b) for ϵ_r'' , which evidences the two relaxations mentioned. When finite-size effects have been considered in less-general models (Bk and C-S) than the complete ones (BKBDVD and CSBDVD), the relaxation MWC frequency is shifted to larger frequencies in comparison with PL predictions, as expected from the increase of both the electrical conductivity and the width of the condensation layer, the shift being larger for the C-S approach [14]. But when all the effects are incorporated into the theory, we do observe a relaxation frequency of the global MW process smaller than those of simpler models and even below the PL prediction in the CSBDVD case (nearly one order of magnitude lower for CSBDVD as compared to C-S). This striking behavior is surely linked to the decrease in the diffusion coefficient of counterions associated to the increased viscosity close to the particles: It was shown in Refs. [14,44] that the MWC relaxation frequency of the condensate is proportional to the diffusion coefficient of the counterions.

In Figs. 7(a) and 7(b) we display the real and imaginary parts of the dynamic mobility and in Figs. 7(c) and 7(d) the real and imaginary part of the complex relative electric permittivity, respectively, as a function of frequency for three salt-free colloids with different counterion radii: $R = 0.358$ nm (Na⁺), $R = 0.331$ nm (K⁺), and H⁺ ($R = 0.282$ nm) according to the CSBDVD approach with $a = 25$ nm,

$\sigma = -40.0 \mu\text{C}/\text{cm}^2$, and $\phi = 0.2$. The closeness between bulk diffusion coefficients of Na⁺ and K⁺ counterions justifies the proximity between their predictions in all the properties analyzed in Fig. 7. It is the larger bulk diffusion coefficient of the counterion H⁺ that is responsible for the deviation observed with respect to the rest of results. The mobility peak of the real part of the dynamic mobility takes place at larger frequencies than those of the rest of ions, as it is well known when a Maxwell-Wagner polarization process relaxes (here again there are two MW relaxation processes, MWO and MWC, very close in frequency giving rise to the global response observed). This fact is more evident in Fig. 7(d), where the MW relaxation frequency is given exactly by the frequency of the maximum of ϵ_r'' . Note the separation of nearly one decade in frequency between these relaxation frequencies for the different ions evaluated. The overall behavior of the CSBDVD model when the counterion radius is changed is the one predicted even for the standard PL model. Only quantitative differences are expected in a comparison between such models according to the effects of the nonhomogeneous viscosity not included in the PL model.

Finally, in Figs. 8(a) and 8(d) we show 3D plots of the real part of the dynamic mobility and the imaginary part of the complex relative electric permittivity, respectively, versus frequency and surface charge density according to the PL model. A similar study for the BKBDVD model is found in Figs. 8(b) and 8(e) and another one for the CSBDVD model in Figs. 8(c) and 8(f). Apart from some quantitative differences already discussed in previous figures between the models, there is a particular behavior of the BKBDVD model for ϵ_r'' in Fig. 8(e) which makes the difference with the other two models. It has to do with the shift trend of the MW relaxation frequency of the overall process: In these figures, it is demonstrated that the sensitivity of the BKBDVD model to surface charge variations is more significant than in the rest of the models. In particular, the MW relaxation frequency increases very notably when the charge density is raised above approximately $-30 \mu\text{C}/\text{cm}^2$. The same arguments apply to the real part of the dynamic mobility in Fig. 8(b). In contrast, plots of the PL and CS predictions [Figs. 8(a) and 8(c) or Figs. 8(d) and 8(f)] show similar qualitative behaviors.

In summary, the Bikerman-like approaches studied in this work have the aim of giving a first comparison with the Carnahan-Starling results due to the simpler mathematical tasks necessary for the numerical resolution of the electrokinetic equations in comparison with the huge difficulties found when it comes to solve the more exact Carnahan-Starling approach. In any case, both approaches coincide in predicting a relaxation frequency shift with the increase of surface charge density. The surprising feature is that the simpler standard PL model also reflects similar behavior to the general CSBDVD model, and this unexpected result brings some additional support to the somewhat reviled standard PL model due to its significant simplifications.

VI. CONCLUSIONS

A general electrokinetic cell model for concentrated salt-free colloids has been developed that generalizes previous works focused on finite-ion-size effects in order to get a more

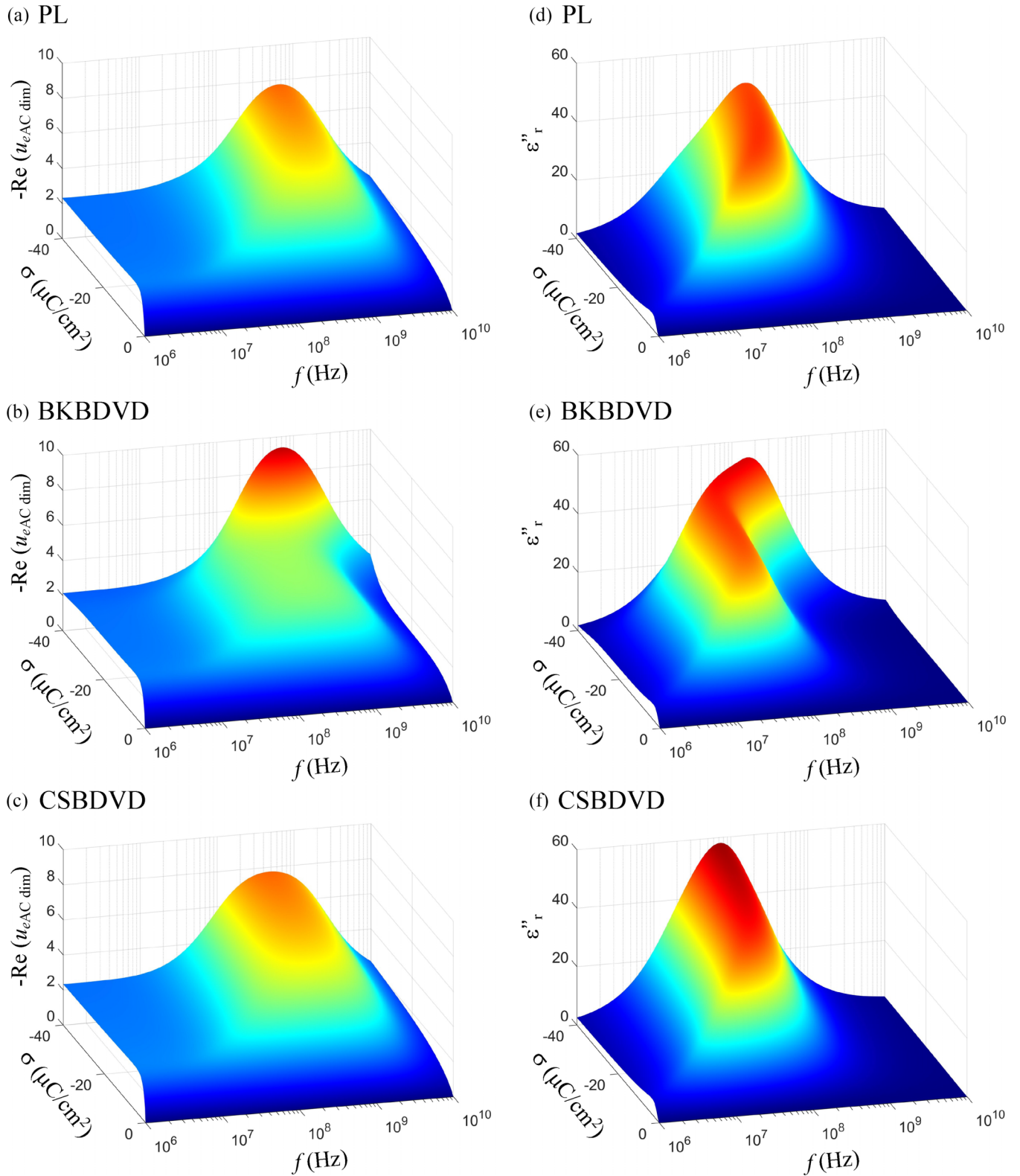


FIG. 8. Real part of the dimensionless dynamic mobility, and imaginary part of the complex relative permittivity as a function of frequency and surface charge density for a salt-free colloid according to PL [(a) and (d)], BKBDVD [(b) and (e)], and CSBDVD [(c) and (f)] with $R = 0.358$ nm (Na^+), $a = 25$ nm, $\phi = 0.2$, and $\epsilon_{ri} = 20$.

realistic insight of the electrokinetic and dielectric response of these systems. Recent studies have revealed that ion finite size not only leads to excluded counterion volume, but equally important are the nonhomogeneous effective permittivity of the solution and the related Born and dielectrophoretic forces acting on the counterions, as well as nonhomogeneous viscosity and counterion diffusion coefficient, dependent on the local counterion concentration. In this work for the first time we have accounted for all these aspects in the case of salt-free nanoparticle suspensions of arbitrary concentration or surface charge. The new model includes a newly developed concentration-viscosity dependence, in an attempt to overcome the limitations of previous viscosity models like that of Batchelor and Green, which underestimate the solution viscosity for the very concentrated counterion conditions that take place in the counterion condensation region very close to highly charged particle surfaces. The calculations are applied to dc electrophoretic mobility and electrical conductivity and to ac mobility and dielectric dispersion. Very significant changes are found in comparison to previous finite-size effects investigation. First, the increase of the dc mobility at high particles charges and particle concentrations, a classically unexpected effect that had been predicted for concentrated salt-free colloids when finite-size effects were considered, is no longer maintained according to the most general approach. Second, the huge mobility maximum in frequency of the real part of the dynamic (or ac) mobility on the relaxation of the Maxwell-Wagner processes changes

dramatically when the most general theory is used. In fact, it is found that the mobility maxima fall to values similar to those of the simple classical pointlike ions models, although the global Maxwell-Wagner relaxation peak shifts to smaller frequencies when viscosity effects and corresponding retarding effects on ionic transport are considered. Finally, it is confirmed that the Born and dielectrophoretic effects linked to the consideration of a nonhomogeneous effective solution permittivity are of minor importance in comparison with the new viscosity effects. In this respect, the predictions are dependent on the choice of the hard-sphere hydrodynamic viscosity model used, and our choice has been an approach that previously demonstrated its ability in explaining the experimental observations on the rheology of moderately concentrated silica colloids. We expect that all these new results may help in better understanding the electrokinetic response of these systems, interesting not only from the fundamental point of view but also when the focus is placed on some applications related to the micro-nanofluidic industry.

ACKNOWLEDGMENTS

Financial support of this investigation through Grant No TED2021-131855BI00, funded by MCIN/AEI/10.13039/501100011033 and Unión Europea NextGenerationEU/PRTR, and Grant No. PID2021-127427NB-I00, funded by MCIN/AEI/10.13039/501100011033 and by “ERDF A way of making Europe,” is acknowledged.

APPENDIX A: DERIVATION OF AUXILIARY FUNCTIONS FOR THE LINEAR PERTURBATION SCHEME

The function $S(r)$ in Eq. (41) is defined by:

$$S(r) = \left\{ \frac{1}{\Lambda(r)} - \frac{3z^2 e^2 \Phi n^0(r) V_c}{8\pi R \epsilon_0 \epsilon_{rs} k_B T [1 + 2\Phi n^0(r) V_c]^2} \right\}^{-1} = \frac{1}{1 + \Upsilon(r) + \Xi(r)}, \quad (A1)$$

where the $\Lambda(r)$ function was defined in Ref. [14] by:

$$\Lambda(r)_{CS} = \frac{1 - 4\varphi^0(r) + 6\varphi^0(r)^2 - 4\varphi^0(r)^3 + \varphi^0(r)^4}{1 + 4\varphi^0(r) + 4\varphi^0(r)^2 - 4\varphi^0(r)^3 + \varphi^0(r)^4}, \quad (A2)$$

$$\Lambda(r)_{Bk} = 1 - \left[\frac{\varphi^0(r)}{p} \right], \quad (A3)$$

being the $\Upsilon(r)$ function defined by Eqs. (14) and (15) for the C-S and Bk approaches, respectively, and the $\Xi(r)$ function by Eq. (16). Equation (42) is obtained by assuming for the nonequilibrium case a similar dependence with counterion concentration as that shown in equilibrium for the effective electrical permittivity [see Eq. (8)]:

$$\epsilon_e(\vec{r}, t) = \epsilon_e^0(r) + \delta\epsilon_e(\vec{r}) \exp(-j\omega t) = \epsilon_s \left\{ \frac{1 + 2\Phi [n^0(r) + \delta n(\vec{r}) \exp(-j\omega t)] V_c}{1 - \Phi [n^0(r) + \delta n(\vec{r}) \exp(-j\omega t)] V_c} \right\}. \quad (A4)$$

In obtaining Eqs. (43) and (44), use has been made of a similar first-order perturbation scheme for the nonequilibrium modified Simha function $S(\vec{r}, t)$ in terms of the nonequilibrium counterion concentration $n(\vec{r}, t) = n^0(r) + \delta n(\vec{r}) \exp(-j\omega t)$:

$$\eta(\vec{r}, t) = \eta^0(r) + \delta\eta(\vec{r}) \exp(-j\omega t) = \eta_s \left[1 + \frac{5}{2} n(\vec{r}, t) V_c S(\vec{r}, t) \right], \quad (A5)$$

$$S(\vec{r}, t) = S^0(r) + \delta S(\vec{r}) \exp(-j\omega t), \quad (A6)$$

$$S(\vec{r}, t) = \frac{4\{1 - [n(\vec{r}, t) V_c]^{7/3}\}}{4\{1 + [n(\vec{r}, t) V_c]^{10/3}\} - 25 n(\vec{r}, t) V_c \{1 + [n(\vec{r}, t) V_c]^{4/3}\} + 42 [n(\vec{r}, t) V_c]^{5/3}}, \quad (A7)$$

$$\delta S(\vec{r}) = Q(r) \delta n(\vec{r}), \quad (A8)$$

where the $S(\vec{r}, t)$ function is admitted to maintain an analogous form as in equilibrium [see Eq. (34) for comparison] but in terms of the above-mentioned counterion concentration $n(\vec{r}, t)$, and by its substitution in Eq. (A5), operating we have:

$$\eta(\vec{r}, t) = \eta^0(r) + \delta\eta(\vec{r}) \exp(-j\omega t) = \eta^0(r) + \frac{5}{2}\eta_s V_c [n^0(r)\delta S(\vec{r}) + S^0(r)\delta n(\vec{r})] \exp(-j\omega t), \quad (\text{A9})$$

from which Eq. (43) can be obtained, where the auxiliary $Q(r)$ function has been defined by:

$$Q(r) = -\frac{7 S^0(r) n^0(r)^{4/3} V_c^{7/3}}{3\{1 - [n^0(r) V_c]^{7/3}\}} - S^0(r) \frac{\frac{40}{3} n^0(r)^{7/3} V_c^{10/3} - 25 V_c \{1 + \frac{7}{3} [n^0(r) V_c]^{4/3}\} + 70 n^0(r)^{2/3} V_c^{5/3}}{4\{1 + [n^0(r) V_c]^{10/3}\} - 25 n^0(r) V_c \{1 + [n^0(r) V_c]^{4/3}\} + 42 [n^0(r) V_c]^{5/3}}. \quad (\text{A10})$$

The auxiliary functions of the linearized continuity equation (49) are

$$\mathbb{J}(r) = \left\{ -\frac{2}{r} h(r) + \frac{ze}{\lambda^0(r)} \frac{d\phi(r)}{dr} - \frac{4\pi R^3}{\lambda^0(r)} \varepsilon_e^0(r) \left[\frac{\varepsilon_i - \varepsilon_e^0(r)}{\varepsilon_i + 2\varepsilon_e^0(r)} \right] \left[\frac{d^2\Psi^0(r)}{dr^2} \frac{dY(r)}{dr} + \frac{d\Psi^0(r)}{dr} \frac{d^2Y(r)}{dr^2} \right] \right. \\ \left. + \frac{4\pi R^3}{\lambda^0(r)} \frac{d\Psi^0(r)}{dr} \frac{d^2\Psi^0(r)}{dr^2} M(r) J(r) \right\} \left[\frac{dn^0(r)}{dr} \right], \quad (\text{A11})$$

$$f(r) = -\frac{4\pi R^3}{\lambda} \varepsilon_e^0(r) \left[\frac{\varepsilon_i - \varepsilon_e^0(r)}{\varepsilon_i + 2\varepsilon_e^0(r)} \right] \left\{ \left[-\frac{1}{r^3} \frac{d\Psi^0(r)}{dr} + \frac{1}{r^2} \frac{d^2\Psi^0(r)}{dr^2} \right] \frac{dY(r)}{dr} + \frac{1}{r^2} \frac{d\Psi^0(r)}{dr} \frac{d^2Y(r)}{dr^2} \right\}, \quad (\text{A12})$$

$$y(r) = -\frac{4\pi R^3}{\lambda} \varepsilon_e^0(r) \left[\frac{\varepsilon_i - \varepsilon_e^0(r)}{\varepsilon_i + 2\varepsilon_e^0(r)} \right] \frac{1}{r} \frac{d\Psi^0(r)}{dr} \frac{dY(r)}{dr}, \quad (\text{A13})$$

$$\zeta(r) = \frac{4\pi R^3}{\lambda} \frac{d\Psi^0(r)}{dr} \frac{d^2\Psi^0(r)}{dr^2} \frac{M(r) J(r)}{r^2}, \quad (\text{A14})$$

and the auxiliary $M(r)$ and $J(r)$ functions are defined by:

$$M(r) = \frac{\varepsilon_i^2 - 2\varepsilon_i \varepsilon_e^0(r) - 2\varepsilon_e^0(r)^2}{[\varepsilon_i + 2\varepsilon_e^0(r)]^2}, \quad (\text{A15})$$

$$J(r) = -\frac{3 \varepsilon_{rs} \varepsilon_0 \Phi V_c ze n^0(r) S(r) [\phi(r) - Y(r)]}{k_B T [1 - \Phi n^0(r) V_c]^2}. \quad (\text{A16})$$

The equation regarding the third-order derivative of the potential (50) also requires of auxiliary functions that can be found as follows:

$$A(r) = -\frac{z^2 e^2}{k_B T} \left(\left[\frac{1}{\varepsilon_e^0(r)} \frac{dn^0(r)}{dr} - \frac{n^0(r)}{\varepsilon_e^0(r)^2} \frac{d\varepsilon_e^0(r)}{dr} \right] [\phi(r) - Y(r)] S(r) + \frac{n^0(r)}{\varepsilon_e^0(r)} \left\{ \left[\frac{d\phi(r)}{dr} - \frac{dY(r)}{dr} \right] S(r) + [\phi(r) - Y(r)] \frac{dS(r)}{dr} \right\} \right), \quad (\text{A17})$$

$$B(r) = \frac{1}{\varepsilon_e^0(r)^2} \left[\frac{d\varepsilon_e^0(r)}{dr} \right]^2 \frac{dY(r)}{dr} - \frac{1}{\varepsilon_e^0(r)} \left[\frac{d^2\varepsilon_e^0(r)}{dr^2} \frac{dY(r)}{dr} + \frac{d\varepsilon_e^0(r)}{dr} \frac{d^2Y(r)}{dr^2} \right], \quad (\text{A18})$$

$$C(r) = -\frac{1}{\varepsilon_e^0(r)^2} \frac{d\varepsilon_e^0(r)}{dr} \frac{dJ(r)}{dr} \frac{d\Psi^0(r)}{dr} + \frac{1}{\varepsilon_e^0(r)} \left[\frac{d^2J(r)}{dr^2} \frac{d\Psi^0(r)}{dr} + \frac{dJ(r)}{dr} \frac{d^2\Psi^0(r)}{dr^2} \right], \quad (\text{A19})$$

$$D(r) = -\frac{1}{\varepsilon_e^0(r)^2} \frac{d\varepsilon_e^0(r)}{dr} J(r) \left[\frac{d^2\Psi^0(r)}{dr^2} + \frac{2}{r} \frac{d\Psi^0(r)}{dr} \right] + \frac{1}{\varepsilon_e^0(r)} \left\{ \frac{dJ(r)}{dr} \left[\frac{d^2\Psi^0(r)}{dr^2} + \frac{2}{r} \frac{d\Psi^0(r)}{dr} \right] \right. \\ \left. + J(r) \left[\frac{d^3\Psi^0(r)}{dr^3} - \frac{2}{r^2} \frac{d\Psi^0(r)}{dr} + \frac{2}{r} \frac{d^2\Psi^0(r)}{dr^2} \right] \right\}. \quad (\text{A20})$$

Use has also been made of the general pressure function perturbation $\delta P(\vec{r}) = \chi(r)(\vec{E} \cdot \hat{r})$, the expression for $\chi(r)$ being

$$\chi(r) = -\eta^0(r) r \left[\frac{d^3 h(r)}{dr^3} + \frac{3}{r} \frac{d^2 h(r)}{dr^2} - \frac{2}{r^2} \frac{dh(r)}{dr} + \frac{2}{r^3} h(r) \right] + \rho_{el}^0(r) Y(r) + j\omega \rho_s \left[u_e r - h(r) - r \frac{dh(r)}{dr} \right] - r \frac{d\eta^0}{dr}(r) \frac{d^2 h}{dr^2}(r), \quad (\text{A21})$$

in order to calculate the hydrodynamic stress tensor and hydrodynamic force acting on the unit cell. The latter Eq. (A21) has been obtained by integrating the Navier-Stokes (N-S) Eq. (28) to derive a full solution of the pressure function perturbation where the linear perturbation scheme, the symmetry conditions, and the incompressibility condition for the fluid described in Eqs. (29), (36)–(44) have been used.

Regarding the derivation of the boundary condition (62), we begin by considering that, since the net electric charge within the unit cell is zero, there is no net electric force acting on it. We need to consider only the hydrodynamic force \vec{F}_h . As the net force is in the direction of the field \vec{E} , the equation of motion for the unit cell in such direction is then given (without vector notation) by:

$$\rho_s \int_0^\pi \int_a^b \frac{d}{dt} \{ [(\delta\vec{u})_r \cos \theta - (\delta\vec{u})_\theta \sin \theta + u_e E] e^{-j\omega t} \} 2\pi r^2 \sin \theta \, dr \, d\theta + \rho_p \frac{4}{3} \pi a^3 \frac{d}{dt} [u_e E e^{-j\omega t}] = F_h \quad (\text{A22})$$

$$F_h = \int_0^\pi [\sigma_{rr} \cos \theta - \sigma_{r\theta} \sin \theta]_{r=b} 2\pi b^2 \sin \theta \, d\theta, \quad (\text{A23})$$

where σ_{rr} and $\sigma_{r\theta}$ are the normal and tangential components of the stress tensor:

$$\begin{aligned} \sigma_{rr} &= -P^0 - \delta P e^{-j\omega t} + 2\eta^0(r) \frac{\partial(\delta\vec{u})_r}{\partial r} e^{-j\omega t} \\ &= -P^0 - \chi E e^{-j\omega t} \cos \theta + 4\eta^0(r) \left[\frac{h}{r^2} - \frac{1}{r} \frac{dh}{dr} \right] E e^{-j\omega t} \cos \theta, \end{aligned} \quad (\text{A24})$$

$$\sigma_{r\theta} = \eta^0(r) \left[\frac{1}{r} \frac{\partial(\delta\vec{u})_r}{\partial \theta} + \frac{\partial(\delta\vec{u})_\theta}{\partial r} - \frac{(\delta\vec{u})_\theta}{r} \right] e^{-j\omega t} = \eta^0(r) \frac{d^2 h}{dr^2} E e^{-j\omega t} \sin \theta. \quad (\text{A25})$$

Substituting in Eq. (A24) the above $\chi(r)$ function [Eq. (A21)], the hydrodynamic force in Eq. (A23) can be obtained as:

$$\begin{aligned} F_h &= \frac{4}{3} \pi b^3 \eta^0(b) E e^{-j\omega t} \left\{ \frac{d^3 h}{dr^3}(b) + \frac{1}{b} \frac{d^2 h}{dr^2}(b) - \frac{6}{b^2} \frac{dh}{dr}(b) + \frac{6}{b^3} h(b) \right. \\ &\quad \left. + \frac{1}{\eta^0(b)} \frac{d\eta^0}{dr}(b) \frac{d^2 h}{dr^2}(b) - \frac{j\omega \rho_s}{\eta^0(b)} \left[u_e - \frac{h(b)}{b} - \frac{dh}{dr}(b) \right] - \frac{\rho_{el}^0(b) Y(b)}{b\eta^0(b)} \right\}. \end{aligned} \quad (\text{A26})$$

Evaluating the left side of Eq. (A22) we also have:

$$\begin{aligned} \rho_s \int_0^\pi \int_a^b \frac{d}{dt} \{ [(\delta\vec{u})_r \cos \theta - (\delta\vec{u})_\theta \sin \theta + u_e E] e^{-j\omega t} \} 2\pi r^2 \sin \theta \, dr \, d\theta + \rho_p \frac{4}{3} \pi a^3 \frac{d}{dt} [u_e E e^{-j\omega t}] \\ = \frac{4}{3} \pi b^3 \eta^0(b) E e^{-j\omega t} \left(-\frac{j\omega \rho_s}{\eta^0(b)} \left\{ u_e \left[(1 - \phi) + \frac{\rho_p}{\rho_s} \phi \right] - 2 \frac{h(b)}{b} \right\} \right). \end{aligned} \quad (\text{A27})$$

Equating Eq. (A26) and Eq. (A27), finally leads to:

$$\frac{d^3 h}{dr^3}(b) + \frac{1}{b} \frac{d^2 h}{dr^2}(b) - \frac{6}{b^2} \frac{dh}{dr}(b) + \frac{6}{b^3} h(b) - \frac{j\omega \rho_s}{\eta^0(b)} \left[\frac{h(b)}{b} - u_e \frac{(\rho_p - \rho_s)}{\rho_s} \phi - \frac{dh}{dr}(b) \right] + \frac{1}{\eta^0(b)} \frac{d\eta^0}{dr}(b) \frac{d^2 h}{dr^2}(b) = \frac{\rho_{el}^0(b) Y(b)}{b\eta^0(b)},$$

which is the aforementioned Eq. (62), related to the force acting on the cell.

APPENDIX B: CALCULATION OF THE COMPLEX ELECTRICAL CONDUCTIVITY

The cell-averaged electric current density is expressed as:

$$\begin{aligned} \langle \vec{i}(\vec{r}, t) \rangle &= \frac{1}{V_{\text{cell}}} \oint_{S_b} \vec{r} \vec{i}(\vec{r}, t) \cdot \hat{r} \, dS_b \\ &= \frac{1}{V_{\text{cell}}} \oint_{S_b} \vec{r} \left\{ z e n^0(r) \delta \vec{v}(\vec{r}) e^{-j\omega t} + j\omega [\varepsilon_e^0(r) \vec{\nabla} \delta \Psi(\vec{r}) + \vec{\nabla} \Psi^0(r) \delta \varepsilon_e(\vec{r})] e^{-j\omega t} \right\} \cdot \hat{r} \, dS_b \\ &= \frac{1}{V_{\text{cell}}} \oint_{S_b} \vec{r} \left(z e n^0(r) \left\{ \delta \vec{u}(\vec{r}) - \frac{1}{\lambda^0(r)} \vec{\nabla} \delta \mu(\vec{r}) + \frac{2\pi R^3}{\lambda^0(r)} \varepsilon_e^0(r) \left[\frac{\varepsilon_i - \varepsilon_e^0(r)}{\varepsilon_i + 2\varepsilon_e^0(r)} \right] \vec{\nabla} \left[2 \frac{d\Psi^0(r)}{dr} \hat{r} \cdot \vec{\nabla} \delta \Psi(\vec{r}) \right] \right. \right. \\ &\quad \left. \left. + \frac{2\pi R^3}{\lambda^0(r)} M(r) \vec{\nabla} \left[\frac{d\Psi^0(r)}{dr} \right]^2 \delta \varepsilon_e(\vec{r}) \right\} e^{-j\omega t} + j\omega [\varepsilon_e^0(r) \vec{\nabla} \delta \Psi(\vec{r}) + \vec{\nabla} \Psi^0(r) \delta \varepsilon_e(\vec{r})] e^{-j\omega t} \right) \cdot \hat{r} \, dS_b \end{aligned} \quad (\text{B1})$$

and then

$$\begin{aligned}
\langle \vec{i}(\vec{r}, t) \rangle = & \left(\frac{1}{V_{\text{cell}}} \oint_{S_b} \vec{r} [zen^0(r) \delta \vec{u}(\vec{r})] \cdot \hat{r} dS_b - \frac{1}{V_{\text{cell}}} \oint_{S_b} \vec{r} \left[zen^0(r) \frac{\vec{\nabla} \delta \mu(\vec{r})}{\lambda^0(r)} \right] \cdot \hat{r} dS_b \right. \\
& + \frac{1}{V_{\text{cell}}} \oint_{S_b} \vec{r} \left\{ zen^0(r) \frac{2\pi R^3}{\lambda^0(r)} \varepsilon_e^0(r) \left[\frac{\varepsilon_i - \varepsilon_e^0(r)}{\varepsilon_i + 2\varepsilon_e^0(r)} \right] \vec{\nabla} \left[2 \frac{d\Psi^0(r)}{dr} \hat{r} \cdot \vec{\nabla} \delta \Psi(\vec{r}) \right] \right\} \cdot \hat{r} dS_b \\
& + \frac{1}{V_{\text{cell}}} \oint_{S_b} \vec{r} \left\{ zen^0(r) \frac{2\pi R^3}{\lambda^0(r)} M(r) \vec{\nabla} \left[\frac{d\Psi^0(r)}{dr} \right]^2 \delta \varepsilon_e(\vec{r}) \right\} \cdot \hat{r} dS_b \\
& \left. + \frac{j\omega}{V_{\text{cell}}} \oint_{S_b} \vec{r} \left[\varepsilon_e^0(r) \vec{\nabla} \delta \Psi(\vec{r}) + \vec{\nabla} \Psi^0(r) \delta \varepsilon_e(\vec{r}) \right] \cdot \hat{r} dS_b \right) e^{-j\omega t}. \tag{B2}
\end{aligned}$$

By using Eqs. (36), (37), (38), (41), and (42), some of the latter surface integrals can be evaluated with the help of the following results:

$$\oint_{S_b} \vec{r} [zen^0(r) \delta \vec{u}(\vec{r})] \cdot \hat{r} dS_b = -2ze n^0(b) h(b) \oint_{S_b} (\vec{E} \cdot \hat{r}) \hat{r} dS_b, \tag{B3}$$

$$\oint_{S_b} \vec{r} \left[zen^0(r) \frac{\vec{\nabla} \delta \mu(\vec{r})}{\lambda^0(r)} \right] \cdot \hat{r} dS_b = -\frac{z^2 e^2 n^0(b)^2}{\lambda^0(b)} b \frac{d\phi}{dr}(b) \oint_{S_b} (\vec{E} \cdot \hat{r}) \hat{r} dS_b, \tag{B4}$$

$$\oint_{S_b} \vec{r} [\varepsilon_e^0(r) \vec{\nabla} \delta \Psi(\vec{r})] \cdot \hat{r} dS_b = -\varepsilon_e^0(b) b \frac{dY}{dr}(b) \oint_{S_b} (\vec{E} \cdot \hat{r}) \hat{r} dS_b, \tag{B5}$$

$$\oint_{S_b} (\vec{E} \cdot \hat{r}) \hat{r} dS_b = \frac{4}{3} \pi b^2 \vec{E}. \tag{B6}$$

Also, it is easy to prove that

$$\begin{aligned}
& \oint_{S_b} \vec{r} \left\{ zen^0(r) \frac{2\pi R^3}{\lambda^0(r)} \varepsilon_e^0(r) \left[\frac{\varepsilon_i - \varepsilon_e^0(r)}{\varepsilon_i + 2\varepsilon_e^0(r)} \right] \vec{\nabla} \left[2 \frac{d\Psi^0(r)}{dr} \hat{r} \cdot \vec{\nabla} \delta \Psi(\vec{r}) \right] \right\} \cdot \hat{r} dS_b \\
& = bzen^0(b) \frac{2\pi R^3}{\lambda^0(b)} \varepsilon_e^0(b) \left[\frac{\varepsilon_i - \varepsilon_e^0(b)}{\varepsilon_i + 2\varepsilon_e^0(b)} \right] (-2) \frac{d^2\Psi^0}{dr^2}(b) \frac{dY}{dr}(b) \oint_{S_b} (\vec{E} \cdot \hat{r}) \hat{r} dS_b, \tag{B7}
\end{aligned}$$

as well as

$$\begin{aligned}
& \oint_{S_b} \vec{r} \left\{ zen^0(r) \frac{2\pi R^3}{\lambda^0(r)} M(r) \vec{\nabla} \left[\frac{d\Psi^0(r)}{dr} \right]^2 \delta \varepsilon_e(\vec{r}) \right\} \cdot \hat{r} dS_b \\
& = -\frac{2b z^2 e^2 n^0(b)^2}{k_B T} \frac{2\pi R^3}{\lambda^0(b)} M(b) \frac{d\Psi^0}{dr}(b) \frac{d^2\Psi^0}{dr^2}(b) \frac{3\varepsilon_{rs}\varepsilon_0 \Phi V_c}{[1 - \Phi n^0(b) V_c]^2} S(b) [\phi(b) - Y(b)] \oint_{S_b} (\vec{E} \cdot \hat{r}) \hat{r} dS_b = 0 \tag{B8}
\end{aligned}$$

and

$$\oint_{S_b} \vec{r} [\vec{\nabla} \Psi^0(r) \delta \varepsilon_e(\vec{r})] \cdot \hat{r} dS_b = -\frac{ze b n^0(b)}{k_B T} \frac{d\Psi^0}{dr}(b) \frac{3\varepsilon_{rs}\varepsilon_0 \Phi V_c}{[1 - \Phi n^0(b) V_c]^2} S(b) [\phi(b) - Y(b)] \oint_{S_b} (\vec{E} \cdot \hat{r}) \hat{r} dS_b = 0. \tag{B9}$$

Substituting all the latter results into Eq. (B2) we obtain:

$$\begin{aligned}
\langle \vec{i}(\vec{r}, t) \rangle = & \left\{ \frac{z^2 e^2 n^0(b)}{\lambda^0(b)} \frac{d\phi}{dr}(b) - zen^0(b) \frac{2h(b)}{b} - j\omega \varepsilon_e^0(b) \frac{dY}{dr}(b) \right. \\
& \left. - 2ze \frac{2\pi R^3}{\lambda^0(b)} n^0(b) \varepsilon_e^0(b) \left[\frac{\varepsilon_i - \varepsilon_e^0(b)}{\varepsilon_i + 2\varepsilon_e^0(b)} \right] \frac{d^2\Psi^0}{dr^2}(b) \frac{dY}{dr}(b) \right\} \vec{E} e^{-j\omega t} = K^*(\omega) (-\vec{\nabla} \Psi(\vec{r}, t)), \tag{B10}
\end{aligned}$$

and, finally,

$$K^*(\omega) = \left\{ \frac{z^2 e^2 n^0(b)}{\lambda^0(b)} \frac{d\phi}{dr}(b) - zen^0(b) \frac{2h(b)}{b} - j\omega \varepsilon_e^0(b) \frac{dY}{dr}(b) - \frac{4ze\pi R^3}{\lambda^0(b)} n^0(b) \varepsilon_e^0(b) \left[\frac{\varepsilon_i - \varepsilon_e^0(b)}{\varepsilon_i + 2\varepsilon_e^0(b)} \right] \frac{d^2\Psi^0}{dr^2}(b) \frac{dY}{dr}(b) \right\} \frac{b}{Y(b)}, \tag{B11}$$

where we have made use of Eqs. (B6) and (70).

- [1] T. Palberg, Crystallization kinetics of colloidal model suspensions: Recent achievements and new perspectives, *J. Phys.: Condens. Matter* **26**, 333101 (2014).
- [2] G. S. Manning, Counterion condensation on charged spheres, cylinders, and planes, *J. Phys. Chem. B* **111**, 8554 (2007).
- [3] G. S. Manning, A counterion condensation theory for the relaxation, rise, and frequency dependence of the parallel polarization of rodlike polyelectrolytes, *Eur. Phys. J. E* **34**, 39 (2011).
- [4] H. Ohshima, Ion size effect on counterion condensation around a spherical colloidal particle in a salt-free medium containing only counterions, *Colloid Polym. Sci.* **296**, 1293 (2018).
- [5] D. A. J. Gillespie, J. E. Hallett, O. Elujoba, A. F. Che Hamzah, R. M. Richardson, and P. Bartlett, Counterion condensation on spheres in the salt-free limit, *Soft Matter* **10**, 566 (2014).
- [6] H. Ohshima, Electrokinetic phenomena in a dilute suspension of spherical colloidal particles in a salt-free medium, *Colloids Surf., A* **222**, 207 (2003).
- [7] F. Carrique, E. Ruiz-Reina, F. J. Arroyo, M. L. Jiménez, and Á. V. Delgado, Dielectric response of a concentrated colloidal suspension in a salt-free medium, *Langmuir* **24**, 11544 (2008).
- [8] E. Ruiz-Reina, F. Carrique, and L. Lechuga, DC electrophoresis and viscosity of realistic salt-free concentrated suspensions: Non-equilibrium dissociation-association processes, *J. Colloid Interface Sci.* **417**, 60 (2014).
- [9] A. V. Delgado, F. Carrique, R. Roa, and E. Ruiz-Reina, Recent developments in electrokinetics of salt-free concentrated suspensions, *Curr. Opin. Colloid Interface Sci.* **24**, 32 (2016).
- [10] J. J. López-García and J. Horno, Poisson-Boltzmann description of the electrical double layer including ion size effects, *Langmuir* **27**, 13970 (2011).
- [11] R. Roa, F. Carrique, and E. Ruiz-Reina, Ion size effects on the electrokinetics of salt-free concentrated suspensions in ac fields, *J. Colloid Interface Sci.* **387**, 153 (2012).
- [12] J. Hoffmann and D. Gillespie, Ion correlations in nanofluidic channels: Effects of ion size, valence, and concentration on voltage- and pressure-driven currents, *Langmuir* **29**, 1303 (2013).
- [13] J.-S. Sin and U.-H. Kim, Ion size effect on electrostatic and electroosmotic properties in soft nanochannels with pH-dependent charge density, *Phys. Chem. Chem. Phys.* **20**, 22961 (2018).
- [14] F. Carrique, E. Ruiz-Reina, F. J. Arroyo, M. L. Jiménez, S. Ahualli, and A. V. Delgado, Electrokinetic and dielectric response of a concentrated salt-free colloid: Different approaches to counterion finite-size effects, *Phys. Rev. E* **105**, 064604 (2022).
- [15] N. F. Carnahan and K. E. Starling, Equation of state for nonattracting rigid spheres, *J. Chem. Phys.* **51**, 635 (1969).
- [16] J. Bikerman, XXXIX. Structure and capacity of electrical double layer, *London, Edinburgh, Dublin Philos. Mag. J. Sci.* **33**, 384 (1942).
- [17] J. J. López-García, J. Horno, and C. Grosse, Differential capacitance of the diffuse double layer at electrode-electrolyte interfaces considering ions as dielectric spheres: Part I. binary electrolyte solutions, *J. Colloid Interface Sci.* **496**, 531 (2017).
- [18] J. J. López-García, J. Horno, and C. Grosse, Transport properties in nanochannels: Ionic size-, permittivity-, and viscosity-related effects, *J. Phys. Chem. C* **124**, 10764 (2020).
- [19] J. J. López-García, J. Horno, and C. Grosse, Ionic size, permittivity, and viscosity-related effects on the electrophoretic mobility: A modified electrokinetic model, *Phys. Rev. Fluids* **4**, 103702 (2019).
- [20] T. Boublík, Hard-sphere equation of state, *J. Chem. Phys.* **53**, 471 (1970).
- [21] G. Mansoori, N. F. Carnahan, K. Starling, and T. Leland Jr, Equilibrium thermodynamic properties of the mixture of hard spheres, *J. Chem. Phys.* **54**, 1523 (1971).
- [22] G. Batchelor and J. Green, The determination of the bulk stress in a suspension of spherical particles to order c^2 , *J. Fluid Mech.* **56**, 401 (1972).
- [23] E. Ruiz-Reina and F. Carrique, Electroviscous effect of concentrated colloidal suspensions in salt-free solutions, *J. Phys. Chem. C* **111**, 141 (2007).
- [24] R. Simha, A treatment of the viscosity of concentrated suspensions, *J. Appl. Phys.* **23**, 1020 (1952).
- [25] J. Happel, Viscosity of suspensions of uniform spheres, *J. Appl. Phys.* **28**, 1288 (1957).
- [26] S. Kuwabara, The forces experienced by randomly distributed parallel circular cylinders or spheres in a viscous flow at small Reynolds numbers, *J. Phys. Soc. Jpn.* **14**, 527 (1959).
- [27] M. Z. Bazant, M. S. Kilic, B. D. Storey, and A. Adjari, Towards an understanding of induced-charge electrokinetics at large applied voltages in concentrated solutions, *Adv. Colloid Interface Sci.* **152**, 48 (2009).
- [28] D. Gillespie, A review of steric interactions of ions: Why some theories succeed and others fail to account for ion size, *Microfluid Nanofluid* **18**, 717 (2015).
- [29] Á. V. Delgado, *Interfacial Electrokinetics and Electrophoresis* (CRC Press, Boca Raton, N. York, 2001), Vol. 106.
- [30] J. J. López-García, J. Horno, and C. Grosse, Influence of the finite size and effective permittivity of ions on the equilibrium double layer around colloidal particles in aqueous electrolyte solution, *J. Colloid Interface Sci.* **428**, 308 (2014).
- [31] E. Nightingale, Jr, Phenomenological theory of ion solvation. effective radii of hydrated ions, *J. Phys. Chem.* **63**, 1381 (1959).
- [32] S. Gavryushov, Electrostatics of B-DNA in NaCl and CaCl₂ solutions: ion size, interionic correlation, and solvent dielectric saturation effects, *J. Phys. Chem. B* **112**, 8955 (2008).
- [33] S. Samavat, F. Carrique, E. Ruiz-Reina, W. Zhang, and P. M. Williams, Dynamic viscosity of colloidal silica suspensions at low and high volume fractions, *J. Colloid Interface Sci.* **537**, 640 (2019).
- [34] H. Eilers, Die viskositäts-konzentrationsabhängigkeit kolloider systeme in organischen lösungsmitteln, *Kolloid Z.* **102**, 154 (1943).
- [35] M. Mooney, The viscosity of a concentrated suspension of spherical particles, *J. Colloid Sci.* **6**, 162 (1951).
- [36] A. Einstein, Berichtigung zu meiner arbeit: Eine neue bestimmung der moleküldimensionen, *Ann. Phys.* **339**, 591 (1911).
- [37] H. Ohshima, Dynamic electrophoretic mobility of a soft particle, *J. Colloid Interface Sci.* **233**, 142 (2001).
- [38] F. Carrique, E. Ruiz-Reina, F. J. Arroyo, and Á. V. Delgado, Cell model of the direct current electrokinetics in salt-free concentrated suspensions: The role of boundary conditions, *J. Phys. Chem. B* **110**, 18313 (2006).
- [39] H. Ohshima, *Electrical Phenomena at Interfaces and Biointerfaces: Fundamentals and Applications in Nano-, Bio-, and Environmental Sciences* (John Wiley & Sons, New Jersey, 2012).

- [40] E. K. Zholkovskij, J. H. Masliyah, V. N. Shilov, and S. Bhattachaljee, Electrokinetic phenomena in concentrated disperse systems: General problem formulation and spherical cell approach, *Adv. Colloid Interface Sci.* **134-135**, 279 (2007).
- [41] R. O'Brien, D. Cannon, and W. Rowlands, Electroacoustic determination of particle size and zeta potential, *J. Colloid Interface Sci.* **173**, 406 (1995).
- [42] F. Carrique, E. Ruiz-Reina, R. Roa, F. J. Arroyo, and Á. V. Delgado, Ionic coupling effects in dynamic electrophoresis and electric permittivity of aqueous concentrated suspensions, *Colloids Surf., A* **541**, 195 (2018).
- [43] H. Ohshima, Electrophoretic mobility of a spherical colloidal particle in a salt-free medium, *J. Colloid Interface Sci.* **248**, 499 (2002).
- [44] R. Roa, F. Carrique, and E. Ruiz-Reina, dc electrokinetics for spherical particles in salt-free concentrated suspensions including ion size effects, *Phys. Chem. Chem. Phys.* **13**, 19437 (2011).
- [45] M. J. Aranda-Rascón, C. Grosse, J. López-García, and J. Horno, Electrokinetics of suspended charged particles taking into account the excluded volume effect, *J. Colloid Interface Sci.* **335**, 250 (2009).